Cell Reports
Methods

Article

Self-amplifying RNA enables rapid, durable, integration-free programming of hiPSCs

Graphical abstract

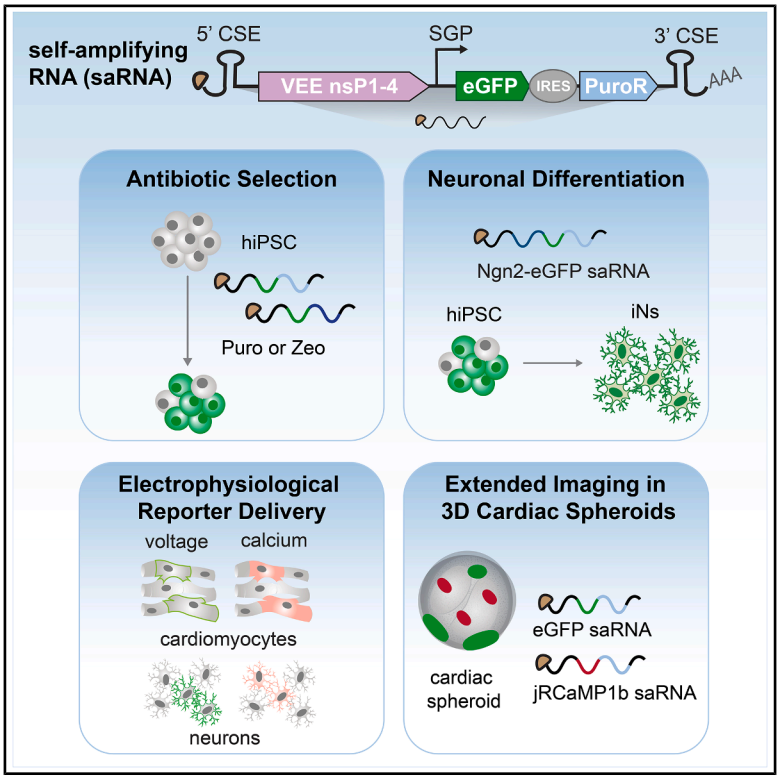

Highlights

- A single saRNA transfection generates durable protein expression in hiPSCs
- saRNA transfection of Ngn2 in hiPSCs results in robust neuronal differentiation
- saRNA delivery of functional reporters is successful in primary and hiPSC-derived cells
- saRNA-based calcium sensor supports extended monitoring of 3D cardiac spheroids

Authors

Catherine M. Della Santina, Deon S. Ploessl, Nicole Lindsay-Mosher, ..., Edward S. Boyden, Kate E. Galloway, Laurie A. Boyer

Correspondence

katiegal@mit.edu (K.E.G.), lboyer@mit.edu (L.A.B.)

In brief

Self-amplifying RNAs (saRNAs) have the potential for rapid, durable, non-integrating delivery of transgenes in human induced pluripotent stem cells. Della Santina et al. show that transcription factors and reporters expressed from saRNA are present for multiple weeks, supporting forward programming to neurons and tracking electrophysiological properties in 3D cardiac spheroids.

Della Santina et al., 2026, Cell Reports Methods 6, 101602
December 21, 2026
https://doi.org/10.1016/j.crmeth.2026.101602

CellPress

Cell Reports Methods

CellPress
OPEN ACCESS

Article

Self-amplifying RNA enables rapid, durable, integration-free programming of hiPSCs

Catherine M. Della Santina,[1,11] Deon S. Ploessl,[2,11] Nicole Lindsay-Mosher,[3] Caroline G. Brown,[1] Mary E. Ehmann,[2] Albert Blanch-Asensio,[2] Eung Chang Kim,[4] Edward S. Boyden,[1,4,5,6,7,8,9,10] Kate E. Galloway,[2,*] and Laurie A. Boyer[1,3,12,*]

[1]Department of Biological Engineering, Massachusetts Institute of Technology (MIT), Cambridge, MA, USA
[2]Department of Chemical Engineering, MIT, Cambridge, MA, USA
[3]Department of Biology, MIT, Cambridge, MA, USA
[4]McGovern Institute for Brain Research, MIT, Cambridge, MA, USA
[5]Department of Media Arts and Sciences, MIT, Cambridge, MA, USA
[6]Department of Brain and Cognitive Sciences, MIT, Cambridge, MA 01239, USA
[7]Koch Institute, MIT, Cambridge, MA, USA
[8]Howard Hughes Medical Institute, Cambridge, MA, USA
[9]Center for Neurobiological Engineering and K. Lisa Yang Center for Bionics at MIT, Cambridge, MA, USA
[10]Yang Tan Collective, MIT, Cambridge, MA, USA
[11]These authors contributed equally
[12]Lead contact
*Correspondence: katiegal@mit.edu (K.E.G.), lboyer@mit.edu (L.A.B.)
https://doi.org/10.1016/j.crmeth.2026.101602

MOTIVATION Current methods to introduce transgenes into human induced pluripotent stem cells (hiPSCs) largely fall into two categories: (1) integrating approaches that have durable expression but are associated with higher risks of off-target effects via insertional mutagenesis, and (2) non-integrating approaches that pose little risk to genomic integrity but have shortened expression periods. Here, we test the ability of self-amplifying RNAs to address these limitations and demonstrate that this integration-free strategy enables persistent expression of transcription factors and functional reporters for weeks and supports forward programming to neurons.

SUMMARY

Genetic modification of human induced pluripotent stem cells (hiPSCs) is a powerful approach to measure and manipulate cellular processes. Conventional genetic engineering of hiPSCs requires laborious processes involving transfection, selection, and expansion that can cause karyotypic abnormalities or transgene silencing during differentiation. The use of self-amplifying RNA (saRNA) is a potential alternative integration-free method for durable expression of transgenes. Here, we used saRNA to deliver transcription factors and functional reporters in hiPSCs and demonstrated that protein expression can persist for weeks. Specifically, saRNA delivery enabled highly efficient forward programming to Ngn2-induced neurons and measurement of functional reporters over time. We show that a single transfection of saRNA-encoded jRCaMP1b in hiPSCs generates sustained reporter expression throughout differentiation to 3D cardiac spheroids, allowing the tracking of cardiomyocyte function and drug responses. Altogether, our systematic analysis shows that saRNA extends transgene expression in hiPSCs, supporting integration-free cell fate programming and functional reporter measurement in clinically relevant model systems.

INTRODUCTION

Genetically encoded reporters and transcription factors are powerful tools for measuring and modifying cellular function and fate. Choice of transgene delivery method sets scalability, durability, and precision in cellular engineering. For example, transient delivery of RNA and plasmids supports rapid, integration-free expression, but it is not well suited for applications that require expression for multiple days or weeks. Alternatively, integration of transgenes using programmable nucleases, transposons, or lentiviruses can support durable expression but requires time-consuming cell line engineering and selection strategies that may affect cellular physiology.[1] Moreover, extended culture as needed for isolation of clonal lines intensifies

Please cite this article in press as: Della Santina et al., Self-amplifying RNA enables rapid, durable, integration-free programming of hiPSCs, Cell Reports Methods (2026), https://doi.org/10.1016/j.crmeth.2026.101602

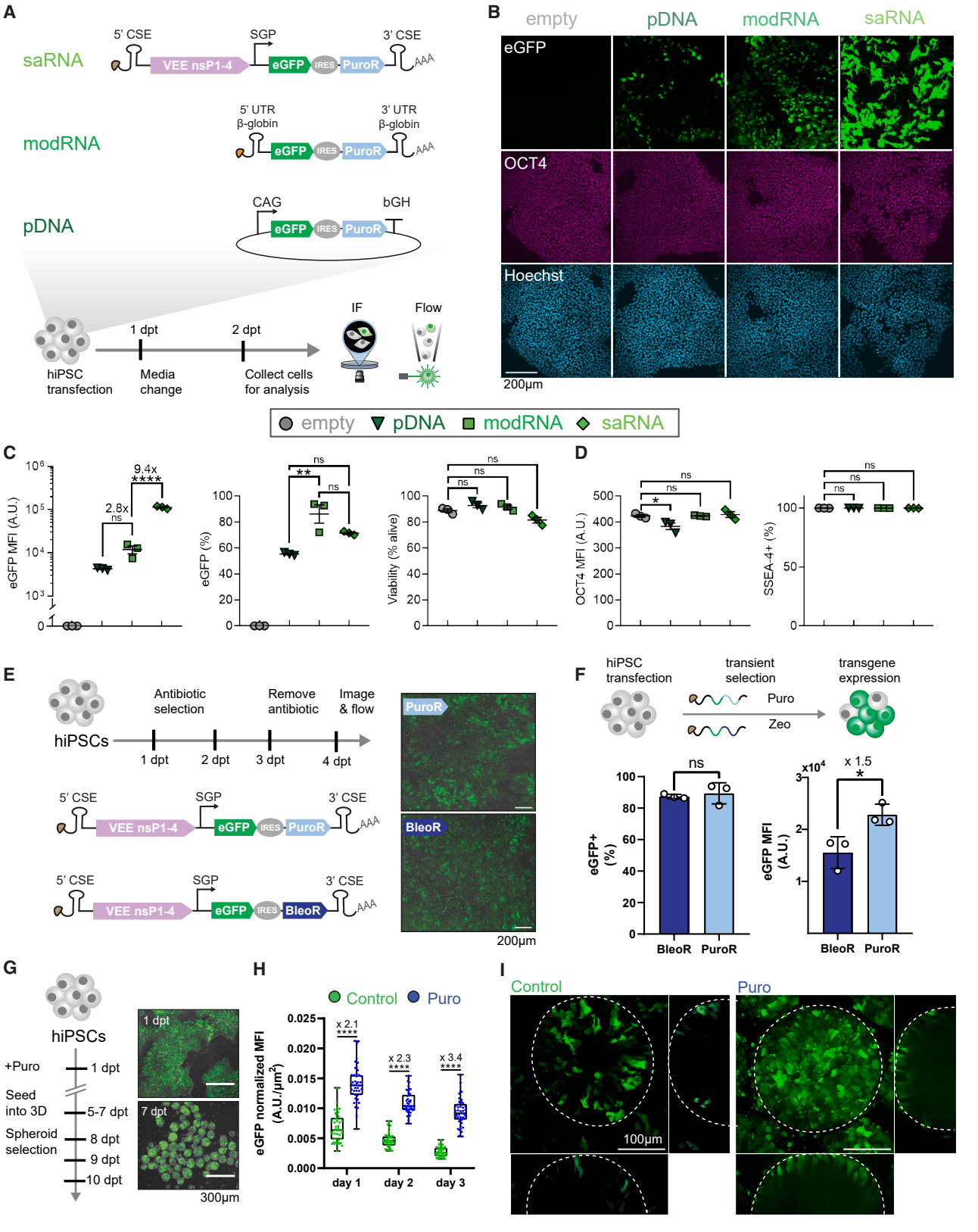

(legend on next page)

Please cite this article in press as: Della Santina et al., Self-amplifying RNA enables rapid, durable, integration-free programming of hiPSCs, Cell Reports Methods (2026), https://doi.org/10.1016/j.crmeth.2026.101602

single-cell bottlenecks that can induce genetic drift, posing a challenge for the generation and comparison of multiple human induced pluripotent stem cell (hiPSC) lines.[2] Although landing-pad hiPSC lines can streamline cell line construction, their initial generation and validation require months, limiting the inherent scalability of this approach.[3] Moreover, integration approaches often result in transgene silencing, limiting the use of hiPSCs for long-term gene expression, therapeutic gene delivery, and other synthetic biology applications.[4,5] While adenoviral-associated virus (AAV) addresses some of these challenges, the small packaging capacity of AAV prevents delivery of large cargoes[6] and production of AAV demands optimization, which can limit scale-up.[4] Modified mRNA (modRNA) supports applications where transient expression is sufficient[1,3,5–9] but require multiple transfections to achieve durable responses, limiting scalability and compromising cell viability.[10–13] In contrast, self-amplifying RNA (saRNA) offers key advantages for delivering transgenes, including higher expression at lower doses and durable expression, yet there has been limited systematic characterization of saRNA as a tool to manipulate hiPSC systems.[14]

Delivery of transgenes using saRNA has been used in applications including protein replacement therapy,[15] hiPSC reprogramming,[16] and inducible gene circuits.[17] saRNAs are derived from positive-strand RNA viruses, encoding the viral conserved sequence elements (CSEs) and non-structural protein genes (nsP1–nsP4) for replication. A transgene can be inserted as a single transcript replicon that facilitates self-replication within the cytoplasm of the host cell (Figure 1A). The endogenous subgenomic promoter (SGP) located upstream of the transgene is separately transcribed by nsP1–nsP4, amplifying transgene transcript levels. Translational applications of saRNAs primarily focus on vaccine development for infectious diseases and cancers.[18] In saRNA-based vaccines, the amplification of transgene expression allows saRNAs to produce similar levels of antigen compared to mRNAs with a fraction of the dose.[19] Because saRNAs are replicated in the cytoplasm and do not contain double-stranded DNA, there is a low risk of genomic integration.[20] Thus, saRNAs could be used more broadly as a tool for durable, scalable, integration-free delivery of transgenes to hiPSCs.[21]

Here, we systematically test saRNA delivery of transgenes in various contexts, demonstrating its use to bridge the gap between rapid, integration-free delivery and durable protein expression in hiPSCs and differentiated cell types. Compared with transfection mediated by either modRNA or plasmid DNA (pDNA), saRNAs induce sustained transgene expression in hiPSCs without affecting cell viability or pluripotency markers. A single transfection of saRNA encoding Ngn2 induces forward programming of hiPSCs into neurons at high efficiency within 6 days. We further demonstrate that the delivery of saRNAs encoding functional reporters can measure critical physiological readouts in hiPSC-derived cardiomyocytes (CMs), cardiac spheroids, and primary mouse hippocampal explants. Sparse labeling allows measurement of cell physiology at single-cell resolution within 3D cardiac spheroids more than 30 days after reporter delivery. Collectively, our work demonstrates that saRNA-mediated delivery enables rapid, durable expression of transgenes, substantially increasing the speed and scalability of hiPSC engineering for a variety of applications.

RESULTS

saRNA delivers efficient, durable transgene expression in hiPSCs

To characterize the potential of saRNAs to deliver sustained expression of transgenes to hiPSCs, we synthesized saRNA derived from components of the Venezuelan equine encephalitis (VEE) virus and compared the expression with modRNA and transient transfection using a standard pDNA vector (Figure 1A).[16] The saRNA encodes the VEE non-structural proteins (nsP1–nsP4) responsible for the amplification of the entire replicon and the transgenic cargo that is downstream of the SGP. Using *in vitro* transcription, we first synthesized the saRNA

Figure 1. saRNA enables sustained transgene expression in 2D and 3D hiPSC cultures

(A–I) Expression from the saRNA confers selection marker resistance without impacting cell viability or pluripotency markers in hiPSCs.

(A) hiPSCs are transfected with equal amounts (by mass) of either saRNA, modRNA, or the pDNA eGFP-IRES-PuroR transgenic cassette. For saRNA, co-opting the alphaviral regulatory sequences drives high expressions of the transgenes located downstream of the subgenomic promoter (SGP). For modRNA, β-globin UTRs enable effective translation of coding mRNA sequences. For pDNA, the CAG promoter and bovine growth hormone (bGH) polyadenylation signal allow efficient expression of transgenes in hiPSCs.

(B) Representative fluorescence microscopy images of hiPSCs fixed at 2 days post-transfection (dpt) with each delivery construct in (A).

(C) Flow cytometry analysis of eGFP expression (MFI [mean fluorescence intensity] measured at 2 dpt in arbitrary units [a.u.] and percentage positive for eGFP are reported as the geometric mean of three biological replicates) and cell viability (percentage of live single cells, reported as the arithmetic mean of three biological replicates); error bars ± SEM (standard error of the mean).

(D) Markers of pluripotency measured by nuclear intensity of OCT4 immunostaining via microscopy as shown in (B), and percentage of SSEA4-positive cells measured by flow cytometry. Data are reported as the mean of three biological replicates; error bars ± SEM.

(E) Puromycin (Puro) or zeocin (Zeo) selection for 2 days enriches saRNA-expressing hiPSCs in 2D monolayers. Scale bars: 200 μm.

(F) Flow cytometry analysis of the percentage of $eGFP^+$ cells and mean eGFP expression at 4 dpt after 2 days of Puro or Zeo selection. Data are reported as the mean of three biological replicates; error bars ± SEM.

(G) saRNA yields sustained, robust expression in 3D cultures. The cells were transfected in 2D hiPSC culture prior to seeding into suspension media for spheroid formation and cultured over 4 days while measuring the fluorescence intensity and spheroid size. Scale bars: 300 μm.

(H) Average eGFP fluorescence per unit area for cultures with and without Puro selection in suspension culture. $n = 45$ per distribution (5 spheroids per image and 3 images per well for 3 total wells).

(I) Maximum-intensity projection of a representative spheroid from non-Puro-treated control and Puro-selected well imaged 5 days after seeding into 3D hiPSC spheroids. Scale bars: 100 μm.

Statistical significance in (C) and (D) was determined using one-way ANOVA with Bonferroni correction for multiple comparisons. Statistical significance in (F) and (H) was determined using Student's *t* test. ns (not significant), $p > 0.05$; $^*p < 0.05$; $^{**}p < 0.01$; $^{***}p < 0.001$; $^{****}p < 0.0001$.

Please cite this article in press as: Della Santina et al., Self-amplifying RNA enables rapid, durable, integration-free programming of hiPSCs, Cell Reports Methods (2026), https://doi.org/10.1016/j.crmeth.2026.101602

encoding an enhanced green fluorescent protein (eGFP) and a puromycin N-acetyltransferase (PuroR) selection cassette, separated by an internal ribosome entry site (IRES) downstream of the SGP (see STAR Methods). We also synthesized modRNA and prepared pDNA encoding the same eGFP-IRES-PuroR cassette (Figure 1A), which allowed us to directly compare across methods. hiPSCs were transfected with equal concentrations by mass of each construct. At 2 days post-transfection (dpt), we compared eGFP signal intensity using fluorescence microscopy (Figure 1B) and quantified expression by flow cytometry (Figure 1C). As expected, both modRNA and saRNA transfected a larger fraction of cells compared with pDNA (Figures 1C andS1). We also observed that saRNA delivery led to the highest transgene expression, whereby the mean level of eGFP expression was 9.4-fold and 26.3-fold greater than those obtained using modRNA or pDNA, respectively (Figures 1B and 1C). We attribute the elevated eGFP levels to the saRNA nsP1–nsP4 replication machinery and resulting RNA amplification.

Because delivery vectors and transgene expression can impact cellular physiology, we next measured hiPSC viability and pluripotency marker expression. At 2 dpt, the cells retained high viability and normal morphology across all three delivery modalities, comparable to the transfection control (Figures 1C andS2). OCT4 immunofluorescence intensity was similar in the saRNA and modRNA conditions, whereas we observed a small reduction in pDNA-transfected cells (Figure 1D). SSEA-4 levels were also similar across delivery methods, as quantified by flow cytometry (Figure 1D).

Given that nucleic acids can induce an immune response, we next compared gene expression in hiPSCs at 24 and 48 h post-transfection in saRNA, modRNA, and untransfected conditions by performing bulk RNA sequencing (Figure S3; Table S2). Consistent with prior work,[22] canonical interferon-stimulated genes including *IFIT1*, *OAS1*, and *MX1*, showed elevated expression after saRNA-mediated transfection relative to modRNA and untransfected conditions. Importantly, saRNA delivery resulted in robust transgene expression without substantially affecting cell viability or the expression of key pluripotency markers and supported robust differentiation.

Applications that require long-term expression such as lineage tracing and library screening may benefit from enriching for a population of cells expressing the transgene of interest. Thus, we generated saRNAs with either puromycin resistance (PuroR) or bleomycin resistance (BleoR) and performed antibiotic selection for 48 h starting at 1 dpt followed by medium replacement without antibiotic (Figure 1E).[1,23,24] After short-term selection, more than 90% of cells expressed eGFP at 4 dpt for both selection schemes. Puromycin treatment generated 1.5-fold higher levels of eGFP than zeocin treatment (Figure 1F). This difference may be due to the efficiency of the resistance enzyme or expression of the resistance cassette. Without antibiotic selection, we observed saRNA-encoded eGFP fluorescence through two passages for at least 7 days (Figure S4C). The observed decrease in fluorescence over time is likely explained by cell division-based dilution and the relative growth advantage of lower- or non-expressing cells. Given the improved enrichment and higher eGFP fluorescence levels of saRNA-expressing hiPSCs using puromycin selection, we used PuroR for subsequent experiments.

Long-term experiments using hiPSCs to generate complex cell assemblies require durable expression of desired transgenes. Moreover, the transfection efficiency of 3D cell clusters is generally low, making delivery a challenge at this stage.[25,26] We next tested whether delivery and antibiotic selection of saRNA in hiPSCs could help overcome this limitation. saRNA-expressing hiPSCs were transfected and selected with puromycin for 7 days, followed by the generation of hiPSC spheroids (Figure 1G).[27] Puromycin selection in suspension culture for 3 days (starting the day after seeding) resulted in high quantities of eGFP-expressing hiPSCs across the cell population (days 2, 3, and 4 after seeding into suspension) (Figure 1H; Figures S2D and S2E). Potentially, modulating the cell seeding density and volume of media can be used to tune spheroid diameter to adjust for cell loss under puromycin selection.[28] In the absence of selection, we observed sparse labeling of cells in spheroids (Figure 1I). The ability to achieve uniform, durable transgene expression or sparse labeling of cells provides flexibility for downstream applications.[28]

saRNA-mediated delivery of Ngn2 efficiently differentiates hiPSCs into neurons

Forward programming of hiPSCs is a rapid, robust method to source rare or difficult-to-isolate patient-specific cells for disease modeling, drug discovery, and cell therapies.[5] For example, overexpression of the neuronal transcription factor Ngn2 rapidly differentiates hiPSCs into induced neurons (iNs).[29,30] Durable expression of Ngn2 improves neuronal purity.[29] As such, Ngn2-hiPSC lines typically use the Tet-ON 3G system, with a doxycycline-inducible Ngn2 transgene integrated into the genome.[7,31] Due to the insertional mutagenesis risk associated with DNA-based delivery, integration-free methods of delivering transcription factors (TFs) may reduce artifacts found in genome engineering and provide a greater safety profile for cell therapy applications.[10] While modRNA-mediated delivery of Ngn2 can drive hiPSC differentiation into iNs, the rapid decay of Ngn2 modRNA requires daily transfections for 10 days, substantially increasing cell stress and the cost and complexity of generating iNs.

To test the ability of saRNA-mediated Ngn2 expression for forward programming hiPSCs into iNs, we synthesized and delivered saRNA encoding Ngn2 and eGFP separated by a Porcine teschovirus-1 2A (P2A) skipping peptide to hiPSCs, which allowed us to correlate Ngn2 expression with eGFP expression (Figure 2A). After transfection, we cultured cells in conditions established for forward programming previously via a Tet-ON Ngn2 hiPSC line.[32] We tested differentiation with and without a 48-h puromycin selection from day 1 to day 3 (Figure 2A). By including the IRES-PuroR element on our construct, we could eliminate untransfected hiPSCs. A transient 48-h puromycin treatment reduced the fraction of untransfected cells, yielding a higher proportion of iNs that formed neurite projections (Figure 2B).

With a single transfection of Ngn2-P2A-eGFP saRNA, we observed neurite projections from eGFP-expressing, puromycin-resistant cells and observed the emergence of neuronal clusters at 6 dpt (Figure 2C). The compact, spherical nuclei of iNs

Please cite this article in press as: Della Santina et al., Self-amplifying RNA enables rapid, durable, integration-free programming of hiPSCs, Cell Reports Methods (2026), https://doi.org/10.1016/j.crmeth.2026.101602

CellPress
OPEN ACCESS

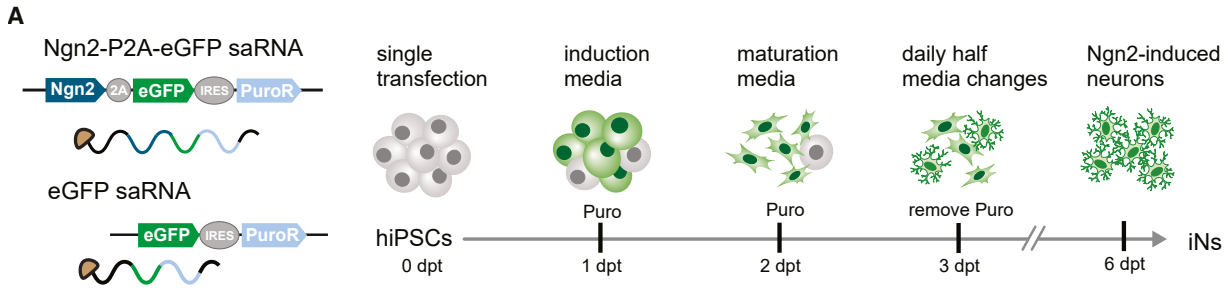

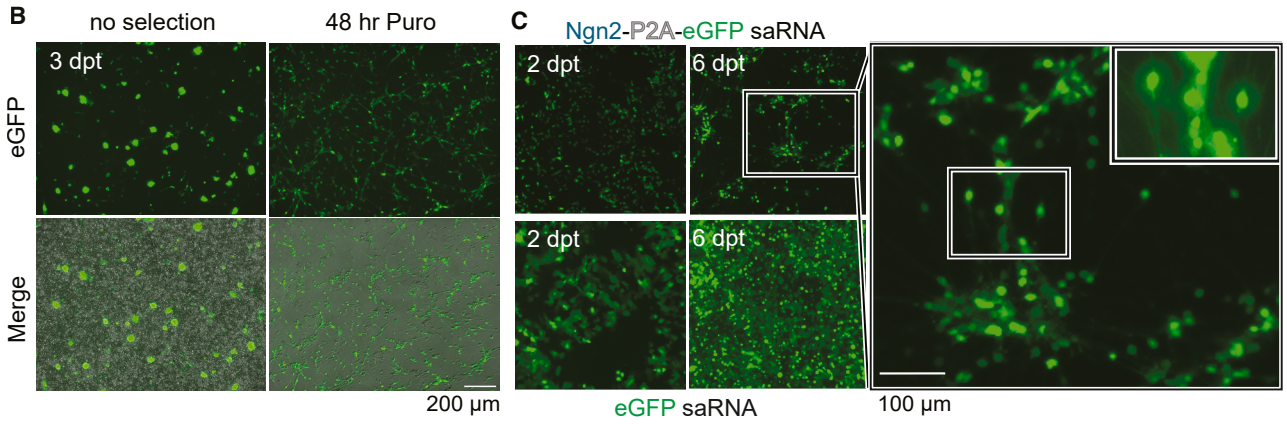

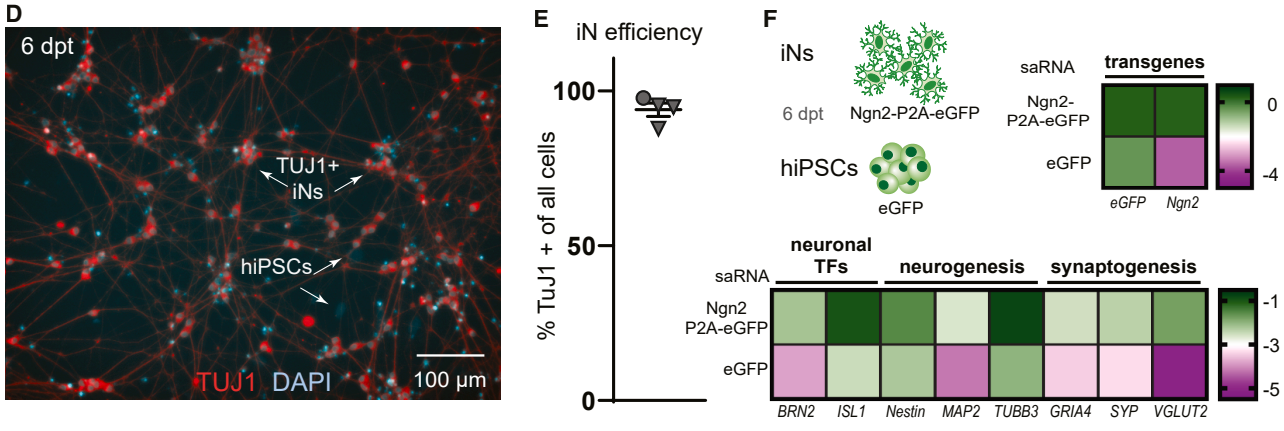

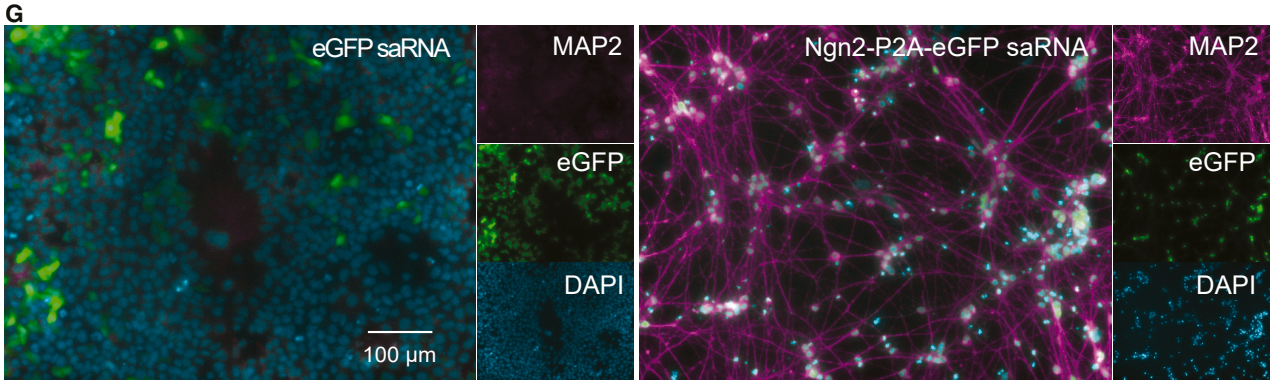

(legend on next page)

Please cite this article in press as: Della Santina et al., Self-amplifying RNA enables rapid, durable, integration-free programming of hiPSCs, Cell Reports Methods (2026), https://doi.org/10.1016/j.crmeth.2026.101602

were readily distinguishable from the larger, elongated nuclei of hiPSCs (SCs) (Figure 2D). To measure differentiation efficiency, we fixed the cells at 6 dpt and quantified the number of cells positive for TUJ1, by immunofluorescence, normalizing to the total number of nuclei. Delivery and selection yielded cultures with more than 90% TUJ1-positive cells, indicating that Ngn2-P2A-eGFP saRNA induces highly efficient differentiation (Figures 2E and S5). Delivery of eGFP saRNA did not yield TUJ1-positive cells despite culture in the same media conditions as the Ngn2-P2A-eGFP saRNA (Figure S6).

To measure the activation of neuronal genes, we compared the expression of key genes in iNs and hiPSCs with eGFP saRNA. As expected, both Ngn2 and eGFP transgenes expressed at 6 dpt, as measured by quantitative reverse-transcription PCR (RT-qPCR). Additionally, while eGFP expressed in both saRNA-transfected cell populations, only the Ngn2-P2A-eGFP saRNA-transfected cells expressed Ngn2 (Figure 2F). Moreover, Ngn2-P2A-eGFP saRNA induced the activation of neuronal genes including *BRN2* and *ISL1* compared with the eGFP-transfected control (Figure 2F). Finally, as measured by immunofluorescence staining at day 6, iNs expressed MAP2, a marker associated with mature neurons (Figure 2G).[33] Collectively, these results indicate that saRNA-mediated delivery of Ngn2 drives highly efficient differentiation of hiPSCs into iNs, that exhibit neuronal morphology, express neuron-associated genes, and are positive for mature neuronal markers, with a single transfection of non-integrating genetic components.

saRNA enables expression of functional reporters in primary and hiPSC-derived cells

Measuring real-time physiological changes in hiPSC-derived cells requires sustained expression of functional reporters. Silencing of genomically integrated transgenes increases during differentiation, limiting the use of genetically encoded tools for functional studies.[9,34,35] On the other hand, delivery of functional reporters using saRNA should resist silencing and allow durable protein expression. To test this idea, we constructed saRNAs encoding functional reporters representing diverse physiological readouts and localization to different subcellular compartments (Figure 3A; Figure S7). Specifically, we synthesized individual saRNAs carrying (1) ASAP5, a voltage reporter that localizes to the cell membrane (Figure 3B), (2) jRCaMP1b, a red-shifted calcium reporter that localizes to the cytosol (Figure 3C), and (3) HyPer7, a redox sensor targeted to mitochondria (Figure S7).[36–38] All dynamic signals were processed with sliding window normalization to remove baseline signal drift during the recording period (Figure S8).

To assess sensor functionality, we tested saRNA-delivered reporters in cell types with robust electrical activity including hiPSC-derived CMs and primary neuronal cells that exhibit characteristic voltage and calcium dynamics. Measuring voltage changes using optical sensors remains challenging because of the fragile nature of the cell membrane, fast kinetics of voltage changes, and low expression of voltage reporters.[39] Thus, we selected ASAP5, a plasma membrane-localized reporter engineered for higher gain and faster onset, enabling critical measurements and comparisons of electrical activity.[37] Next-generation genetically encoded voltage indicators (GEVIs) such as ASAP5 offer a less invasive and higher throughput alternative to patch clamp, with enough spatiotemporal resolution to detect neuron firing and determine the shape of cardiac action potentials, which differ between the atrial, ventricular, and nodal cell types.[40] *In vivo*, ASAP5 shows reduced signal-to-noise ratio and exhibits higher responsivity to action potentials and excitatory postsynaptic potentials compared with previously developed GEVIs. Delivery of saRNA encoding ASAP5 to primary mouse hippocampal cells, including neurons, and hiPSC-derived CMs showed that ASAP5 signal localizes to the membrane (Figures 3B and 3C). As expected, ASAP5 traces appeared as pulses of decreased fluorescence in response to membrane depolarization which showed stochastic activity in neurons and rhythmic patterns in CMs. In CMs, membrane depolarizations coincided with visible membrane contraction, resulting in up to a 10% change in fluorescence over ~1 s (Figure 3B). In addition to the characteristic action potential duration (APD) of cardiac muscle cells, ASAP5 traces exhibit a prolonged plateau phase and slower repolarization time, which reflects the expected enrichment of ventricular CMs in hiPSC differentiation.[41]

ASAP5 signal in mouse hippocampal culture was observed after 30 days *in vitro* and 2 days after saRNA transfection (Figure 3C). At this time point, it is expected that primary hippocampal cultures will have formed network connections and exhibit spontaneous synaptic activity.[42] Within primary mouse hippocampus explant cultures, cells with characteristic neuronal morphology, including small cell bodies and long, branched processes, were visually identified and treated as putative neurons. Consistent with these expectations, we observed intermittent changes in reporter brightness, which confirmed spontaneous electrical activity in neurons as well as reporter responsiveness to depolarization

Figure 2. saRNA-based delivery of Ngn2 efficiently differentiates hiPSCs into iNs

(A) Overview of saRNA-based forward programming of hiPSCs into iNs.

(B) Fluorescence microscopy images of hiPSCs transfected with Ngn2-P2A-eGFP saRNA taken at 3 dpt, with and without 48 h puromycin selection starting at 1 dpt. Scale bars: 200 μm.

(C) Fluorescence microscopy images taken at 2 and 6 dpt during conversion process of hiPSCs into iNs for hiPSCs transfected with either Ngn2-P2A-eGFP (top row) or eGFP saRNA control (bottom row). Scale bars: 100 μm.

(D) Immunofluorescence images (TUJ1, red; DNA, cyan) of hiPSCs transfected with Ngn2-P2A-eGFP saRNA fixed at 6 dpt, with white arrows indicating $TUJ1^+$ iNs and TUJ1-hiPSCs (SCs). Scale bars: 100 μm.

(E) Quantification of the percentage of $TUJ1^+$ cells post-differentiation at 6 dpt, showing a high proportion of iNs. $N = 2$ independent differentiation experiments with 1 and 3 technical replicates (circle and triangles, respectively).

(F) Gene expression analysis of transgenes and neuronal markers, comparing the Ngn2-P2A-eGFP with eGFP saRNA control. Values represent the average of $N = 3$ independent differentiations, normalized to the RPL37A housekeeping gene and $\log_{10}$ transformed.

(G) Immunofluorescence images (MAP2, magenta; eGFP, green; DNA, cyan) of Ngn2-P2A-eGFP and eGFP saRNA control fixed at 6 dpt. Scale bars: 100 μm.

Please cite this article in press as: Della Santina et al., Self-amplifying RNA enables rapid, durable, integration-free programming of hiPSCs, Cell Reports Methods (2026), https://doi.org/10.1016/j.crmeth.2026.101602

CellPress
OPEN ACCESS

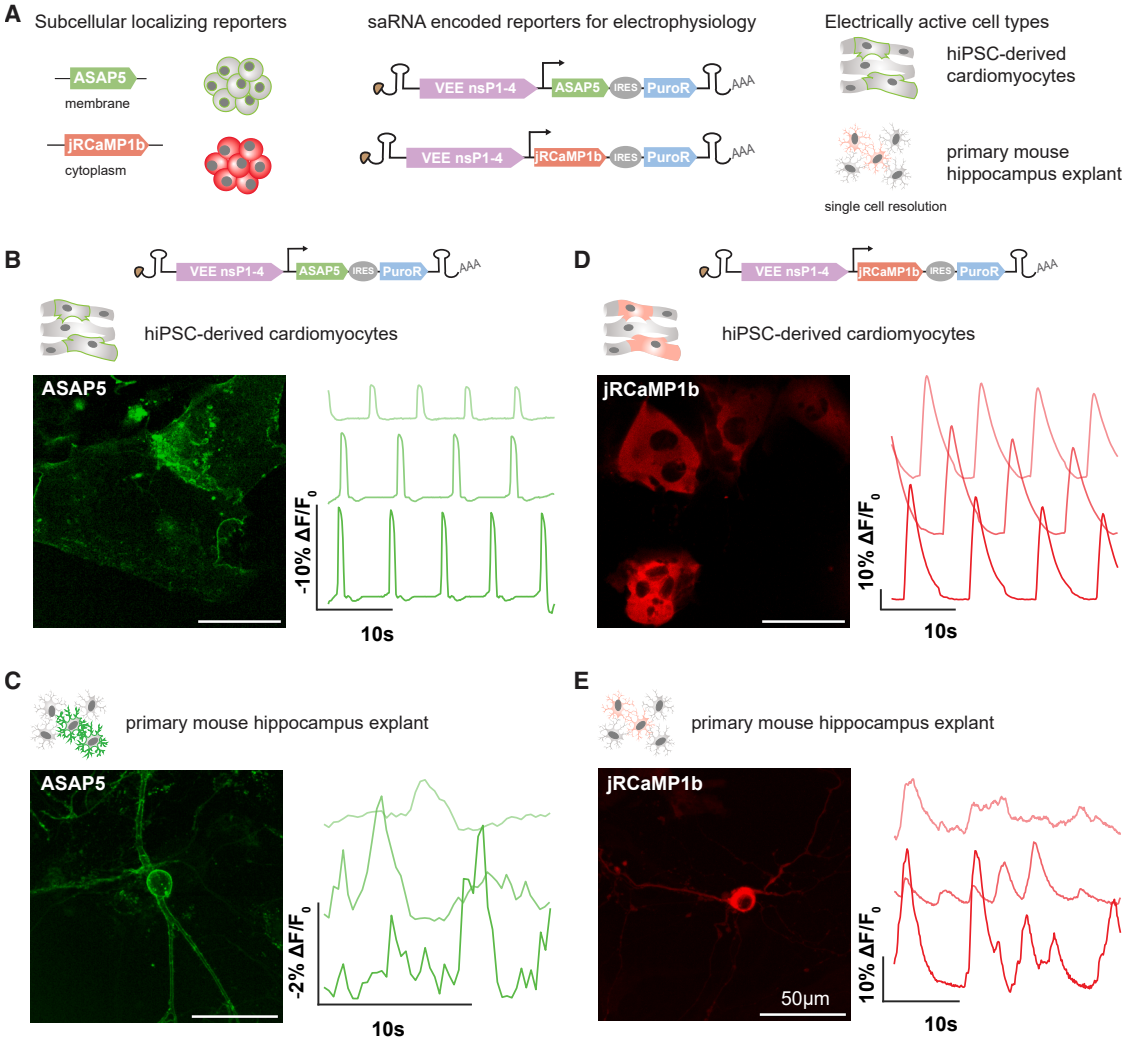

Figure 3. saRNA-encoded functional reporters properly localize in cells and report voltage and calcium dynamics in electrically active cell types

(A) Schematic of saRNA-mediated delivery of subcellular localizing fluorescent reporters to distinct cell types.

(B–E) $n = 3$ representative cells from 3 separate fields of view (FOV) in a single transfected well. All data collection was performed at 2 dpt, using a spinning disk confocal microscope (Yokogawa CSU-W1 confocal scanner unit on a Nikon Eclipse Ti microscope) equipped with a 40×1.15 NA water immersion objective and Zyla PLUS 4.2 Megapixel camera.

(B and C) ASAP5 imaging was performed using 488-nm excitation light and FITC emission filter.

(D and E) jRCaMP1b imaging was performed using 561-nm excitation light and Cy3 emission filter. Fluorescence traces were normalized to a local baseline (F_0) calculated within a sliding window of W frames. For each frame, F_0 was defined as the Pth percentile of the fluorescence values within that window, and the normalized signal is expressed as $\Delta F/F_0 = (|F - F_0|)/F_0$. ASAP5 membrane localized voltage sensor in (B) iPSC-derived cardiomyocytes (CMs) imaged at 10 Hz over 30-s recording period (normalization parameters: W = 25; $p = 50$) and (C) primary mouse hippocampal explant culture at 3.33 Hz for 15 s (normalization parameters: W = 20; $p = 90$). Membrane depolarization events are reported as the negative percent change from baseline fluorescence because ASAP5 exhibits inverse voltage sensitivity where brightness decreases during depolarization. jRCaMP1b cytosolic calcium reporter in (D) iPSC-derived CMs imaged at 10 Hz for 30 s (normalization parameters: W = 100; $p = 10$) and (E) primary mouse hippocampus explant cells imaged at 10 Hz for 30 s (normalization parameters: W = 100; $p = 10$). Scale bars: 50 μm.

events. For three representative cells recorded over 15 s, ASAP5 signal fluctuated by 1%–5% over 1–2 s. These dynamics are consistent with subthreshold synaptic potentials as opposed to full action potentials.[37] Imaging modalities that achieve higher temporal resolution would further allow detection of the sub-millisecond action potentials associated with neurons, offering a potential alternative to more laborious patch-clamp analysis.

To monitor calcium dynamics, we next transfected saRNA encoding jRCaMP1b, a genetically encoded calcium indicator (GECI).[36] Like GEVIs, GECIs allow non-invasive measurement of cellular activity but can be more readily observed on standard imaging setups because of their slower rate of change and higher expression throughout the cytoplasm (as opposed to the cell membrane). Delivery of saRNAs encoding jRCaMP1b to

Please cite this article in press as: Della Santina et al., Self-amplifying RNA enables rapid, durable, integration-free programming of hiPSCs, Cell Reports Methods (2026), https://doi.org/10.1016/j.crmeth.2026.101602

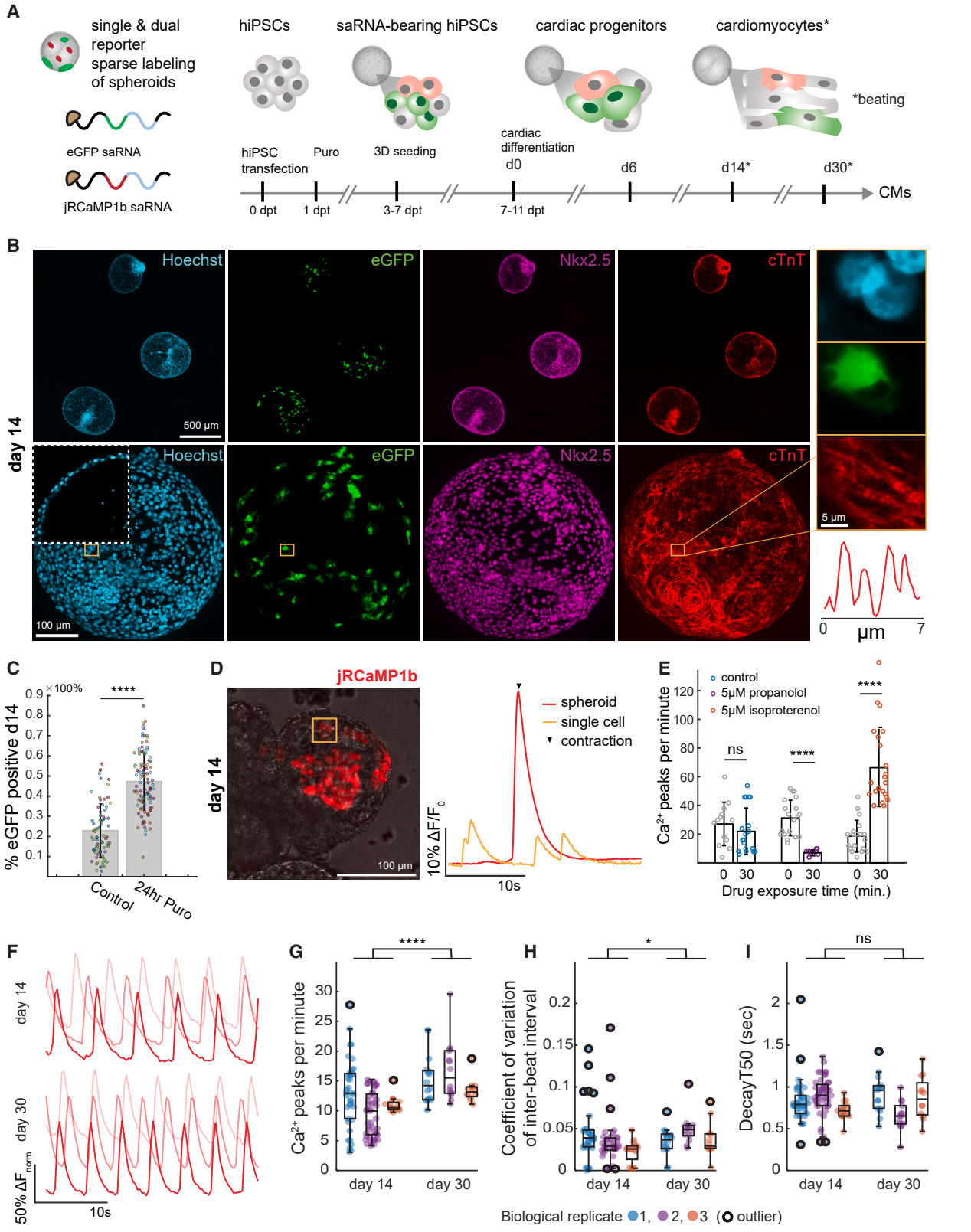

(legend on next page)

Please cite this article in press as: Della Santina et al., Self-amplifying RNA enables rapid, durable, integration-free programming of hiPSCs, Cell Reports Methods (2026), https://doi.org/10.1016/j.crmeth.2026.101602

hiPSC-derived CMs and primary mouse hippocampus explants enabled measurement of calcium transients in single cells (Figures 3D and 3E). As with ASAP5, CMs displayed characteristic rhythmic patterns of calcium signaling (Figure 3D), and neurons showed stochastic activity across cells like those reported for GECIs (Figure 3E).[43] Across three representative cells, jRCaMP1b signal fluctuated by a maximum of 8%–15% over an average of 6.67 s in CMs, with a faster increase in fluorescence lasting 1.13 s and longer return to baseline in 5.53 s. This is consistent with spontaneous calcium transients in immature hiPSC-derived CMs recorded at room temperature, where reduced sarcoplasmic reticulum function and slower ion channel kinetics prolong rise and decay times.[44–46] Recordings at 37°C showed more rapid kinetics and are consistent with measurements of Fluo-4, a calcium-sensitive dye (Figure S9). The observed amplitudes fall within the range expected for red-shifted GECIs.[36] In putative mouse neurons, jRCaMP1b fluorescence increased by up to 31%, and a single peak lasted at most 5.86 s. These amplitudes and kinetics are consistent with previous reports of jRCaMP1b in cultured neurons, where transient durations ranged from 1 to 10 s[36,47] The relatively slow decay of the signal suggests that these neurons exhibit prolonged intracellular calcium elevations, potentially reflecting sustained spontaneous activity under these experimental conditions. We also demonstrated that saRNA can deliver mitochondrially targeted HyPer7, a genetically encoded fluorescent H_2O_2 sensor that can be readout in diverse cell types (Figure S7). Thus, saRNA offers a versatile platform for rapid, non-integrating delivery and durable measurement of functional reporters in primary and differentiated cell types using conventional fluorescence microscopy.

saRNA delivery of reporters enables functional readouts in hiPSC-derived 3D cardiac spheroids

To examine the potential of saRNA-delivered fluorescent reporters for monitoring hiPSC differentiation in 3D systems, we tested saRNA-encoded protein durability during hiPSC differentiation to cardiac spheroids. Remarkably, saRNA-encoded protein expression persisted throughout differentiation for over 30 days (Figure 4A). We transfected iPSCs with saRNA in 2D culture and selected with puromycin for 5–7 days prior to cardiac differentiation. saRNA-enriched hiPSCs were seeded into spheroids followed by cardiac differentiation using standard protocols (see STAR Methods). We observed beating in eGFP-labeled cardiac spheroids between days 6 and 7 of differentiation with eGFP saRNA. Immunofluorescent staining showed robust expression of the CM marker Nkx2.5 by day 14 of differentiation, including in cells expressing eGFP (Figure 4B). saRNA-treated CMs also exhibited a clear sarcomere banding pattern, evidenced by cardiac troponin T (cTnT) immunofluorescence staining. Using 2D differentiation, we also show that saRNA transfection does not inhibit the differentiation efficiency, as we observed >93% of eGFP-expressing cells overlapped cTnT relative to 88% of eGFP-negative cells by flow cytometry (Figure S10).

We next tested a 24-h puromycin selection step to further enrich cells expressing saRNA-encoded proteins once seeded into suspension. Across replicates, puromycin selection increased the fraction of cells labeled at day 14 (Figure 4C). To maximize expression of the reporter in cTnT-positive cells at day 30, we included this enrichment step for experiments continued to day 30 (Figure 4G) but omitted selection for day 14 measurements (Figures 4D and 4E). The brief additional selection did not affect the generation of robustly beating eGFP-labeled spheroids that were positive for Nkx2.5 and cTnT (Figures S11B and S11C). We also show that eGFP intensity is not correlated with calcein AM, CellROX, MitoView, or cleaved caspase-3 signals, indicating that saRNA-based transgene expression does not have a significant impact on cell viability, oxidative stress, mitochondrial membrane potential, or apoptosis in long-term culture (Figure S12).

Figure 4. saRNA-based fluorescent reporters enable long-term functional readout of calcium dynamics in 3D cardiac spheroids

(A) Overview of saRNA-based reporter delivery to hiPSCs to cardiac spheroid differentiation protocol.

(B) Maximum projections of immunofluorescent images (Hoechst, cyan; eGFP, green; Nkx2.5, magenta; cardiac troponin T [cTnT]; red) of a representative cardiac spheroid expressing saRNA-eGFP fixed at day 14 of differentiation. Top row: 4× magnification, scale bars: 500 μm; Bottom row: 20× magnification, scale bars: 100 μm. Inset with dotted white line shows a single z slice of Hoechst channel, demonstrating chamber formation. Inset with orange border shows a single z slice at 40× magnification, showing banded sarcomere formation in eGFP-positive cells. Scale bars: 5 μm.

(C) Labeling percentage for day 14 cardiac spheroids expressing saRNA-eGFP with and without an initial 24-h puromycin (Puro) selection step after seeding into 3D suspension culture. Each point represents a single spheroid, and each distribution contains two independent differentiations (Control: $n = 77$ from two differentiations with 3 wells each; 24-h Puro: $n = 115$ from two differentiations with 2 wells and 3 wells each). Data are reported as the mean, and error bars represent the standard deviation. $p = 8.25 \times 10^{-25}$, by t test.

(D) (Left) Cardiac spheroid at day 14 of differentiation expressing saRNA-jRCaMP1b. Representative overlay of bright-field and maximum projection of z stack at 561-nm illumination taken at 40× on day 14 of differentiation. (Right) Accompanying 30-s recording of the average change in jRCaMP1b signal measured in a single cell (orange line) at sub-contraction level and across the entire cardiac spheroid (red line) during a contraction, noted with black arrow. Normalized by minimum fluorescence value across the recording period. Scale bars: 100 μm.

(E) Calcium peaks per minute as measured by 30 s recordings of jRCaMP1b signal at 4× magnification with 300 ms exposure time (9 fps) before and after 30-min incubation with 5 μM propranolol or 5 μM isoproterenol compared with control media (from left to right $n = 13$, 20, 20, 14, 19, and 23 beating cardiac spheroids). Data are reported as the mean of all observations; error bars represent the standard deviation. $p = 0.3704$, 3.354×10^{-8}, and 1.022×10^{-8}, by t test.

(F) Representative traces of jRCaMP1b taken at day 14 and day 30 of three independent differentiations. One representative trace is selected per differentiation. Normalized between 0 and 1 to compare temporal parameters.

(G–I) Calcium peaks per minute (G), coefficient of variation of inter-beat interval (H), and time to decay to 50% (Decay T50) of peak brightness (I) for three independent differentiations compared at day 14 and day 30, where $n = 38$, 49, and 16 for day 14 and $n = 16$, 14, and 12 for day 30 across 3 wells each (day 14; $N = 16$ represents one well).

For (G)–(I), data are represented by a boxplot showing the median (line within box), interquartile range/IQR (box), and data points outside of 1.5 × IQR as outliers. Whiskers extend to the most extreme points within 1.5 × IQR. $p = 7.67 \times 10^{-7}$, 0.017, and 0.3771 for (G) –(I) respectively, by Mann-Whitney U test. ns (not significant), $p > 0.05$; *$p < 0.05$; **$p < 0.01$; ***$p < 0.001$; ****$p < 0.0001$.

Please cite this article in press as: Della Santina et al., Self-amplifying RNA enables rapid, durable, integration-free programming of hiPSCs, Cell Reports Methods (2026), https://doi.org/10.1016/j.crmeth.2026.101602

Having demonstrated the maintenance of saRNA-eGFP-expressing spheroids throughout a 30-day 3D differentiation period, we next tested our ability to measure a dynamic physiological reporter in this system. Sparse labeling is particularly valuable for dynamic imaging, such as calcium or voltage signals, where overlapping fluorescence from neighboring cells can obscure spatial resolution.[48] Calcium fluxes directly reflect excitation-contraction coupling and electrophysiological maturity and are a gold-standard functional assay for hiPSC-derived CMs in disease modeling and drug screening contexts.[49,50] Thus, we generated sparsely labeled jRCaMP1b-expressing cardiac spheroids and observed calcium transients during differentiation progression. At day 14, we measured both small, non-contractile fluctuations in single cells and large, contraction-coupled calcium transients across the entire spheroid, plotted as normalized fluorescence intensity ($\Delta F/F_0$) over time (Figure 4D). Cardiac spheroids expressing both eGFP and jRCaMP1b could also be generated by seeding equal numbers of eGFP-transfected and jRCaMP1b-transfected hiPSCs prior to differentiation, making this a flexible method for combining multiple labels without burdening individual cells with more than one transgene (Figure S11D). As proof of concept, we next measured calcium dynamics using jRCaMP1b-expressing CMs in response to well-characterized drugs that disrupt CM function. We added propranolol or isoproterenol, which block or increase calcium influx, respectively, to day 14 cardiac spheroids for 30 min and measured the fluorescence intensity over time. From a single field of view with low magnification, we could segment and extract up to 20 independent calcium recordings per condition to rapidly assess changes in beat rate due to drug treatment. As expected, exposure to propranolol decreased calcium peak number by 77.3% and treatment with isoproterenol increased the calcium peak number by 257%, while the control group showed no statistically significant change (Figures 4E andS13B).

The ability to maintain reporter expression for more than 30 days using saRNA delivery enabled measurement of calcium dynamics in CMs throughout differentiation and maturation (Figures 4F–4I; Figure S13C). To track calcium signaling over a longer observational period, we included 24-h puromycin selection upon seeding into suspension to increase reporter signal at day 30 (Figure S14). We found that the beat rate increased from day 14 to day 30 across three independent differentiations. In a 3D spheroid differentiation system, this difference likely reflects robust coupling and synchronization between cells.[51] Moreover, the coefficient of variation (CV) of the inter-beat interval was slightly higher, on average, on day 30 than on day 14. The narrower distribution on day 30 indicated that there were fewer spheroids with irregular beating patterns observed across the population (Figure 4H). As CMs mature, they develop faster calcium decay kinetics, a key hallmark of functional maturation and efficient excitation-contraction coupling.[52] Despite a higher average number of calcium peaks per minute, we did not observe statistically significant differences in the calcium decay kinetics on day 30 compared with day 14 (Figure 4I). These data are consistent with the known lack of functional maturity of hiPSC-derived CMs, indicating the need for assessing calcium dynamics beyond beat frequency. Although we initially focused on parameters that prioritize experimental throughput to support the idea that saRNA can scale to screening applications, we found that sensor brightness on day 30 is sufficient to capture calcium transients at a 50 Hz frame rate, enabling faster kinetic measurements, including rise time (Figure S11F). Moreover, saRNA-GECIs optimized for fast transient calcium imaging can be used if higher temporal resolution or speed is preferred over the longer-lasting spectral properties of jRCaMP1b. Together, these data demonstrate that saRNA-encoded fluorescent reporters can be used to track dynamic signals over long observational periods with a single non-integrating transfection, greatly expanding the toolkit for non-invasive imaging of biological processes for multiple applications that require extended culture time.

DISCUSSION

We systematically tested saRNA delivery to hiPSCs and primary cells as a flexible tool for durable expression of transgenes in multiple applications. saRNAs generate high protein levels in hiPSCs without compromising their viability, pluripotency, or ability to differentiate. We also show that a single transfection of the saRNA encoding Ngn2 to hiPSCs leads to high efficiency of differentiation into neurons. Moreover, we demonstrate that saRNAs can deliver GEVIs or GECIs to electrically active cell types such as neurons and CMs. Finally, we show that saRNA delivery of jRCaMP1b to hiPSCs allows long-term monitoring of calcium dynamics to assess functional state and response to drug perturbations in cardiac spheroids. Thus, saRNA offers a rapid, efficient method to forward program hiPSCs into neurons and to generate footprint-free fluorescent reporter lines. Together, our data support that saRNA can be broadly used as a highly scalable tool for functional manipulation and observation of hiPSCs and hiPSC-derived cells.

Current methods to introduce genetic payloads to hiPSCs are subject to a major tradeoff between the duration of expression and risk from genomic integration. Non-integrating tools including Sendai virus, episomal vectors, synthetic mRNA, pDNAs, protein transduction, and AAVs pose little risk for unintended genomic integration. However, transient expression from these tools is often insufficient for observing the differentiation processes or longer-term monitoring of disease states.[53] Integrating tools like lentiviruses, retroviruses, CRISPR-Cas9, and transposons are often used to generate stable cell lines, but these methods pose a higher risk of insertional mutagenesis, off-target effects, and genetic drift.[54,55] Leveraging saRNA to facilitate long-term transgene expression obviates the need for the cumbersome and slow pipelines of cellular engineering, enabling more rapid exploration of biological phenomena. The ease with which saRNA tools achieve high-efficiency and long-term transgene delivery serves to democratize stem cell engineering and enables more labs to incorporate biosensors in their measurements of hiPSCs and hiPSC-derived cell types. This will accelerate the rate at which candidate factors and biosensors can be tested across tissue systems, driving the development of next-generation therapies and advancing new discoveries.[56] We evaluated multiple reporters to highlight the flexibility of the platform. Given the common use of reporters that use the green

Please cite this article in press as: Della Santina et al., Self-amplifying RNA enables rapid, durable, integration-free programming of hiPSCs, Cell Reports Methods (2026), https://doi.org/10.1016/j.crmeth.2026.101602

channel, we designed saRNA-based reporters that were compatible for multiplex imaging experiments. While the relative dimness and slower kinetics of the red channel jRCaMP1b reporter may limit observation of rapid calcium transients, our system's flexibility could accommodate GCaMP depending on experimental goals.[36]

We demonstrate the applicability of saRNA to forward program hiPSCs into iNs. *Ngn2*-driven differentiation of hiPSCs yields neurons that can be used for drug screening and cell therapy. Previous work established that forward programming to neurons requires durable expression of Ngn2.[29] As such, Ngn2-hiPSC lines typically use the Tet-ON 3G system, with a doxycycline-inducible Ngn2 transgene integrated into the genome, along with a constitutively expressed transactivator.[7,31] Depending on the syntax of the Tet-ON elements, a single, site-specific integrated copy of Tet-inducible Ngn2 can efficiently differentiate hiPSCs into iNs.[32] However, harnessing the power of diverse hiPSC lines requires scalable methods of engineering neurons, underscoring the value of fast, robust tools. Importantly, as a non-integrating vector with FDA approval for administration to patients,[57] saRNA may offer improved scalability and safety for translating hiPSC-derived neurons as cell therapies. Existing modRNA-based protocols achieve ~70% TUJ1$^+$ cells after 10 days of daily transfections,[58] compared with >90% TUJ1$^+$ cells after 6 days with a single transfection, indicating further improvement. The simple, rapid production of hiPSC-derived iNs at clinically relevant purities via Ngn2 saRNA allows scaling the potential of disease modeling and drug screening with hiPSC-derived cells. Combining saRNA *Ngn2*-driven forward programming with specific small molecules and growth factors may further advance disease modeling by enabling the scalable generation of neuronal subtypes.[59–61]

3D spheroids and organoids have emerged as powerful models for studying human development, diseases, and drug responses, offering a more physiologically relevant alternative to traditional 2D cultures. Their 3D architecture and multicellular complexity replicate key features of native tissues, but these same properties create challenges for gene delivery. This limitation is especially true for non-integrating, transient transfection methods, like lipid-based reagents or electroporation, which fail to deliver payloads within dense, differentiated structures. Thus, introducing genetic tools, such as fluorescent biosensors, earlier in the workflow by manipulating hiPSCs in 2D adherent culture could help overcome this limitation. We demonstrate that saRNA-based delivery achieves sparse sensor labeling with robust and enduring signal in 3D cardiac spheroids with a single transfection prior to differentiation. Because saRNA delivery is highly scalable, its implementation to deliver reporters across many cell lines offers a key advantage for the identification of genotype-specific effects of drug compounds, thereby improving genotype-based stratification of candidates for clinical trials. Moreover, the durable expression of fluorescent reporters avoids repeated dosing, while enabling dynamic measurements for long-term safety studies, a feature lacking in traditional drug screening modalities.[62] Though we initially selected cardiac spheroids as a testbed system to demonstrate the utility of saRNA to construct footprint-free optical reporter lines, we expect this approach to be applicable across multiple tissue types, further augmenting the potential of saRNA as an impactful addition to a researcher's toolbox.[57]

Beyond our demonstrations in forward programming and measuring functional reporters, there remain opportunities to tailor the design of saRNAs for their broadest application. High expression of transgenes supported our testbed applications of Ngn2-based differentiation to neurons and calcium tracing in cardiac spheroids. However, some applications may require precise or controllable levels of proteins. For example, transient expression of the pioneer transcription factor ETV2 in hiPSCs produces more mature endothelial cells compared with sustained overexpression.[63] Moreover, overexpression of some genetic sensors may induce proteotoxic stress, metabolic burden, or other off-target physiological effects.[64] Synthetic biology approaches to control saRNA transgene expression can support tuning of expression. For example, SGP tuning[65] can offer pretranslational control of transgene expression, and fusing trimethoprim (TMP)-responsive degradation domains to the alphaviral non-structural proteins or the transgene product offers posttranslational control.[66] Combining the evolving control mechanisms could further tune output of transgene expression by calibrating initial expression levels and offering inducible degradation of the replication machinery and/or gene product. In theory, multiple transcription factors or combinations of transcription factors and reporters could be encoded on a single saRNA. However, the design rules for larger polycistronic cassettes are not yet defined. Both the exact sequence of the transgenes, their connecting sequences (e.g., IRESs and self-cleaving peptides), and the length of the saRNA may affect transfection and expression. However, the modularity of saRNA-encoded payloads should enable rapid and iterative design testing across combinations of genetic components to optimize performance. While our goal is durable protein expression, we also recognize that direct quantification of RNA levels or kinetics is a next step for understanding the dynamics of these systems.

Innate immune signaling remains an important consideration for saRNA-based delivery platforms. This may be particularly relevant for differentiation protocols that are sensitive to inflammatory signaling or in applications directly focusing on the immune or inflammatory pathways, where saRNA-induced transcriptional responses could confound downstream measurements or cellular phenotypes. Previous works suggest that saRNA-induced inflammatory responses can be mitigated using immune-evasive strategies, including synthesizing saRNA with modified nucleotides,[22] engineering replicons that co-express the E3L dsRNA-binding protein from vaccinia virus,[67,68] and passaging replicons under exogenous interferon stress to evolve saRNAs with attenuated immunogenicity.[69] Thus, these optimizations are expected to further extend the applicability of saRNA as a biological tool.

Collectively, our study shows that using saRNA is a fast, simple, robust, and non-integrating method for transgene delivery, offering a more scalable solution for engineering hiPSCs. With broader adoption of saRNA-based tools in this context, we anticipate accelerated innovations and discoveries across developmental biology, disease research, and drug screening applications.

Limitations of the study

While we demonstrate saRNA-mediated transgene delivery in two hiPSC lines, it is possible that cell lines of different genetic backgrounds would respond differently to saRNA transfection or the resulting high expression of transcription factors or reporters. Additionally, because we were interested in durable expression of protein factors and reporters, we did not directly measure the saRNA replication dynamics within the cells. These data cannot distinguish ongoing saRNA replication from slow decay of a stable transcript or selective expansion of highly expressing cells, and future studies are needed to determine the relationship between saRNA replicon persistence and protein stability. Lastly, while we observed measurable changes during the 30-day maturation window reported in cardiac spheroids, the data presented here likely reflect a relatively early stage of maturation, and much longer longitudinal experiments would be needed to better relate the changes in calcium signaling to CM maturation in this system.

RESOURCE AVAILABILITY

Lead contact

Requests for further information and resources should be directed to and will be fulfilled by the lead contact, Laurie A. Boyer (lboyer@mit.edu).

Materials availability

Plasmids generated in this study have been deposited to Addgene.

Data and code availability

- RNA-sequencing data have been deposited at GEO: GSE334590 and are publicly available as of the date of publication.
- All original code and key flow cytometry and microscopy datasets have been deposited on GitHub at lboyerlab/hiPSC_saRNA_Analysis and https://doi.org/10.5281/zenodo.22014494.
- Any additional information required to reanalyze the data reported in this paper is available from the lead contact upon request.

ACKNOWLEDGMENTS

Research reported in this manuscript was supported by the National Institute of General Medical Sciences of the National Institutes of Health under Health under award number R35-GM143033, by the National Science Foundation under the NSF-CAREER under award number 2339986, by the Air Force Research Laboratory MURI under award FA9550-22-1-0316, and funding from Institute for Collaborative Biotechnologies under cooperative agreement W911NF-19-2-0026 and the Pershing Square Foundation MIND Prize (K.E.G.). This work was also supported by the National Institute of Heart Lung and Blood R01 HL140471 (L.A.B.). The authors thank MIT M-CELS seed funding for supporting this work (K.E.G. and L.A.B.). E.S.B. acknowledges funding from HHMI, Lisa Yang, and NIH R01 AG087374. N.L.-M. acknowledges funding from CIHR (Canadian Institutes of Health Research) Fellowship MFE-200996. The authors also acknowledge the Koch Institute's R.A. Swanson (1969) Biotechnology Center (National Cancer Institute grant P30-CA14051) for technical support, specifically the Microscopy Core and the BioMicro Center Core facilities. The authors thank Nat Wang, Leah Borden, and Dandan Yang for experimental help. Finally, the authors thank Dandan Yang, Nat Wang, Brittany Lende-Dorn, and Maria Castellanos for feedback on the manuscript.

AUTHOR CONTRIBUTIONS

C.M.D.S., D.S.P., K.E.G., and L.A.B. conceived and outlined the project; C.M.D.S., D.S.P., and N.L.-M. conducted flow cytometry and immunofluorescence comparison of saRNA, modRNA, and pDNA; D.S.P. performed molecular cloning, synthesized modRNA and saRNA, and analyzed data; D.S.P., M.E.E, and A.B.-A conducted neuronal differentiations and immunostainings; C.M.D.S. performed transfection, imaging, and analysis of voltage and calcium reporters; E.C.K. prepared primary neural cultures and advised on transfection experiments; C.M.D.S. and C.G.B. performed cardiac spheroid differentiations, imaging, and analysis; C.M.D.S., D.S.P., L.A.B., and K.E.G. wrote and edited the manuscript with input from all authors; L.A.B., K.E.G., and E.S.B. secured funding and supervised the project.

DECLARATION OF INTERESTS

The authors declare no competing interests.

DECLARATION OF GENERATIVE AI AND AI-ASSISTED TECHNOLOGIES IN THE WRITING PROCESS

During the preparation of this work, the authors used ChatGPT GPT-4o to draft initial MATLAB analysis scripts. After using this tool, the authors reviewed and edited the content as needed and take full responsibility for the content of the publication.

STAR★METHODS

Detailed methods are provided in the online version of this paper and include the following:

- KEY RESOURCES TABLE
- EXPERIMENTAL MODEL AND STUDY PARTICIPANT DETAILS
- METHOD DETAILS
  - Molecular cloning
  - *In vitro* transcription
  - Transfection of hiPSCs with saRNA
- QUANTIFICATION OF TRANSFECTION EFFICIENCY, CELL VIABILITY, AND PLURIPOTENCY MARKERS
  - Flow cytometry
  - RNA sequencing and analysis
  - hiPSC suspension spheroid culture
  - Fixation, immunofluorescent staining, and purity quantification of induced neurons (iNs)
  - Quantitative PCR analysis of induced neurons (iNs)
  - Imaging of HyPer7 reporter
  - Voltage and calcium imaging and analysis in 2D cell culture
  - Differentiation of hiPSCs to cardiomyocytes in suspension
  - Fixation and immunofluorescent staining of cardiac spheroids
  - Quantification of labeling percentage in cardiac spheroids
  - Viability and metabolic health assessment in cardiac spheroids
  - Calcium imaging in cardiac spheroids
  - Calculation of calcium peak parameters in cardiac spheroids
  - Assessment of cardiomyocyte differentiation efficiency
- QUANTIFICATION AND STATISTICAL ANALYSIS

SUPPLEMENTAL INFORMATION

Supplementary data related to this article can be found online at https://doi.org/10.1016/j.crmeth.2026.101602.

Received: December 11, 2025
Revised: June 12, 2026
Accepted: August 20, 2026

REFERENCES

1. Bedada, F.B., Thompson, B.R., Mikkila, J.L., Chan, S.S.-K., Choi, S.H., Toso, E.A., Kyba, M., and Metzger, J.M. (2024). Inducing positive inotropy in human iPSC-derived cardiac muscle by gene editing-based activation

of the cardiac α-myosin heavy chain. Sci. Rep. *14*, 3915. https://doi.org/10.1038/s41598-024-53395-4.

2. Peterson, S.E., and Loring, J.F. (2014). Genomic Instability in Pluripotent Stem Cells: Implications for Clinical Applications. J. Biol. Chem. *289*, 4578–4584. https://doi.org/10.1074/jbc.R113.516419.
3. Blanch-Asensio, A., van der Vaart, B., Vinagre, M., Groen, E., Arendzen, C., Freund, C., Geijsen, N., Mummery, C.L., and Davis, R.P. (2023). Generation of AAVS1 and CLYBL STRAIGHT-IN v2 acceptor human iPSC lines for integrating DNA payloads. Stem Cell Res. *66*, 102991. https://doi.org/10.1016/j.scr.2022.102991.
4. Jiang, Z., and Dalby, P.A. (2023). Challenges in scaling up AAV-based gene therapy manufacturing. Trends Biotechnol. *41*, 1268–1281. https://doi.org/10.1016/j.tibtech.2023.04.002.
5. Nicholson, M.W., Ting, C.-Y., Chan, D.Z.H., Cheng, Y.-C., Lee, Y.-C., Hsu, C.-C., Huang, C.-Y., and Hsieh, P.C.H. (2022). Utility of iPSC-Derived Cells for Disease Modeling, Drug Development, and Cell Therapy. Cells *11*, 1853. https://doi.org/10.3390/cells11111853.
6. Marrone, L., Marchi, P.M., and Azzouz, M. (2022). Circumventing the packaging limit of AAV-mediated gene replacement therapy for neurological disorders. Expert Opin. Biol. Ther. *22*, 1163–1176. https://doi.org/10.1080/14712598.2022.2012148.
7. Chen, M., Wang, X., Li, C., Lan, T., Wei, Y., Tang, C., Zhou, X., Zhou, R., Rosa, A., Zheng, X., et al. (2022). Inducible motor neuron differentiation of human induced pluripotent stem cells in vivo. Cell Prolif. *55*, e13319. https://doi.org/10.1111/cpr.13319.
8. Bhagwan, J.R., Collins, E., Mosqueira, D., Bakar, M., Johnson, B.B., Thompson, A., Smith, J.G.W., and Denning, C. (2019). Variable expression and silencing of CRISPR-Cas9 targeted transgenes identifies the AAVS1 locus as not an entirely safe harbour. F1000Res. *8*, 1911. https://doi.org/10.12688/f1000research.19894.2.
9. Cabrera, A., Edelstein, H.I., Glykofrydis, F., Love, K.S., Palacios, S., Tycko, J., Zhang, M., Lensch, S., Shields, C.E., Livingston, M., et al. (2022). The sound of silence: Transgene silencing in mammalian cell engineering. Cell Syst. *13*, 950–973. https://doi.org/10.1016/j.cels.2022.11.005.
10. Tolomeo, A.M., Laterza, C., Grespan, E., Michielin, F., Canals, I., Kokaia, Z., Muraca, M., Gagliano, O., and Elvassore, N. (2021). NGN2 mmRNA-Based Transcriptional Programming in Microfluidic Guides hiPSCs Toward Neural Fate With Multiple Identities. Front. Cell. Neurosci. *15*, 602888. https://doi.org/10.3389/fncel.2021.602888.
11. Contato, A., Gagliano, O., Magnussen, M., Giomo, M., and Elvassore, N. (2022). Timely delivery of cardiac mmRNAs in microfluidics enhances cardiogenic programming of human pluripotent stem cells. Front. Bioeng. Biotechnol. *10*, 871867. https://doi.org/10.3389/fbioe.2022.871867.
12. Kim, S.-M., Lim, M.-S., Lee, E.-H., Jung, S.J., Chung, H.Y., Kim, C.-H., and Park, C.-H. (2017). Efficient Generation of Dopamine Neurons by Synthetic Transcription Factor mRNAs. Mol. Ther. *25*, 2028–2037. https://doi.org/10.1016/j.ymthe.2017.06.015.
13. Ko, S.H., Kang, J.S., Kim, S.-M., Lee, E.-H., and Park, C.-H. (2023). Reduced Cytotoxicity by Repetitive mRNA Transfection in Differentiated Neurons. Int. J. Stem Cells *16*, 117–122. https://doi.org/10.15283/ijsc22125.
14. Vallet, T., and Vignuzzi, M. (2025). Self-Amplifying RNA: Advantages and Challenges of a Versatile Platform for Vaccine Development. Viruses *17*, 566. https://doi.org/10.3390/v17040566.
15. Papukashvili, D., Rcheulishvili, N., Liu, C., Ji, Y., He, Y., and Wang, P.G. (2022). Self-Amplifying RNA Approach for Protein Replacement Therapy. Int. J. Mol. Sci. *23*, 12884. https://doi.org/10.3390/ijms232112884.
16. Yoshioka, N., Gros, E., Li, H.-R., Kumar, S., Deacon, D.C., Maron, C., Muotri, A.R., Chi, N.C., Fu, X.-D., Yu, B.D., and Dowdy, S.F. (2013). Efficient Generation of Human iPS Cells by a Synthetic Self-Replicative RNA. Cell Stem Cell *13*, 246–254. https://doi.org/10.1016/j.stem.2013.06.001.
17. Wagner, T.E., Becraft, J.R., Bodner, K., Teague, B., Zhang, X., Woo, A., Porter, E., Alburquerque, B., Dobosh, B., Andries, O., et al. (2018). Small-molecule-based regulation of RNA-delivered circuits in mammalian cells. Nat. Chem. Biol. *14*, 1043–1050. https://www.nature.com/articles/s41589-018-0146-9.
18. Dailey, G.P., Crosby, E.J., and Hartman, Z.C. (2023). Cancer vaccine strategies using self-replicating RNA viral platforms. Cancer Gene Ther. *30*, 794–802. https://doi.org/10.1038/s41417-022-00499-6.
19. Liu, Y., Li, Y., and Hu, Q. (2023). Advances in saRNA Vaccine Research against Emerging/Re-Emerging Viruses. Vaccines (Basel) *11*, 1142. https://doi.org/10.3390/vaccines11071142.
20. Casmil, I.C., Jin, J., Won, E.-J., Huang, C., Liao, S., Cha-Molstad, H., and Blakney, A.K. (2025). The advent of clinical self-amplifying RNA vaccines. Mol. Ther. *33*, 2565–2582. https://doi.org/10.1016/j.ymthe.2025.03.060.
21. Wagner, A., and Mutschler, H. (2023). Design principles and applications of synthetic self-replicating RNAs. WIREs RNA *14*, e1803. https://doi.org/10.1002/wrna.1803.
22. McGee, J.E., Kirsch, J.R., Kenney, D., Cerbo, F., Chavez, E.C., Shih, T.-Y., Douam, F., Wong, W.W., and Grinstaff, M.W. (2025). Complete substitution with modified nucleotides in self-amplifying RNA suppresses the interferon response and increases potency. Nat. Biotechnol. *43*, 720–726. https://doi.org/10.1038/s41587-024-02306-z.
23. Rashid, M.I., Ito, T., Miya, F., Shimojo, D., Arimoto, K., Onodera, K., Okada, R., Nagashima, T., Yamamoto, K., Khatun, Z., et al. (2023). Simple and efficient differentiation of human iPSCs into contractible skeletal muscles for muscular disease modeling. Sci. Rep. *13*, 8146. https://doi.org/10.1038/s41598-023-34445-9.
24. Harding, J., Vintersten-Nagy, K., Yang, H., Tang, J.K., Shutova, M., Jong, E.D., Lee, J.H., Massumi, M., Oussenko, T., Izadifar, Z., et al. (2024). Immune-privileged tissues formed from immunologically cloaked mouse embryonic stem cells survive long term in allogeneic hosts. Nat. Biomed. Eng. *8*, 427–442. https://doi.org/10.1038/s41551-023-01133-y.
25. Urzì, O., Gasparro, R., Costanzo, E., De Luca, A., Giavaresi, G., Fontana, S., and Alessandro, R. (2023). Three-Dimensional Cell Cultures: The Bridge between In Vitro and In Vivo Models. IJMS *24*, 12046. https://doi.org/10.3390/ijms241512046.
26. Zhang, H., Lee, M.-Y., Hogg, M.G., Dordick, J.S., and Sharfstein, S.T. (2010). Gene Delivery in Three-Dimensional Cell Cultures by Superparamagnetic Nanoparticles. ACS Nano *4*, 4733–4743. https://doi.org/10.1021/nn9018812.
27. Gong, L., Zhang, Y., Zhu, Y., Lee, U., Luo, A.C., Li, X., Wang, X., Chen, D., Pu, W.T., Lin, R.-Z., et al. (2025). Rapid generation of functional vascular organoids via simultaneous transcription factor activation of endothelial and mural lineages. Cell Stem Cell *32*, 1200–1217.e6. https://doi.org/10.1016/j.stem.2025.05.014.
28. Zhu, S., Yin, J., Lu, X., Jiang, D., Chen, R., Cui, K., He, W., Huang, N., and Xu, G. (2025). Influence of experimental variables on spheroid attributes. Sci. Rep. *15*, 9751. https://doi.org/10.1038/s41598-025-92037-1.
29. Muñoz-Estrada, J., Mostafania, A., Halwatura, L., Haghani, A., Jiang, Y., and Meyer, J.G. (2025). Extended NGN2 Expression in iPSCs Dramatically Enhances Purity of Neuronal Cultures. Preprint at bioRxiv. https://doi.org/10.1101/2025.06.20.660764.
30. Zhang, Y., Pak, C., Han, Y., Ahlenius, H., Zhang, Z., Chanda, S., Marro, S., Patzke, C., Acuna, C., Covy, J., et al. (2013). Rapid Single-Step Induction of Functional Neurons from Human Pluripotent Stem Cells. Neuron *78*, 785–798. https://doi.org/10.1016/j.neuron.2013.05.029.
31. Fernandopulle, M.S., Prestil, R., Grunseich, C., Wang, C., Gan, L., and Ward, M.E. (2018). Transcription Factor–Mediated Differentiation of Human iPSCs into Neurons. CP Cell Biology *79*, e51. https://doi.org/10.1002/cpcb.51.
32. Blanch-Asensio, A., Ploessl, D.S., Wang, N.B., Mummery, C.L., Galloway, K.E., and Davis, R.P. (2026). STRAIGHT-IN Dual: a platform for dual, single-copy integrations of DNA payloads and gene circuits into human

induced pluripotent stem cells. Nat. Biomed. Eng., 1–18. https://doi.org/10.1038/s41551-026-01677-9.

33. Soltani, M.H., Pichardo, R., Song, Z., Sangha, N., Camacho, F., Satyamoorthy, K., Sangueza, O.P., and Setaluri, V. (2005). Microtubule-Associated Protein 2, a Marker of Neuronal Differentiation, Induces Mitotic Defects, Inhibits Growth of Melanoma Cells, and Predicts Metastatic Potential of Cutaneous Melanoma. Am. J. Pathol. *166*, 1841–1850. https://doi.org/10.1016/S0002-9440(10)62493-5.

34. Guichardaz, M., Bottini, S., Balmas, E., and Bertero, A. (2024). Overcoming the Silencing of Doxycycline-Inducible Promoters in hiPSC-derived Cardiomyocytes. Open Res. Eur. *4*, 266. https://doi.org/10.12688/openreseurope.19024.1.

35. Durens, M., Baljinnyam, E., Grisanti, L., Hu, R., and Marro, S.G. (2024). An induced pluripotent stem cell line carrying a silencing-resistant calcium reporter allele. Stem Cell Res. *79*, 103455. https://doi.org/10.1016/j.scr.2024.103455.

36. Dana, H., Mohar, B., Sun, Y., Narayan, S., Gordus, A., Hasseman, J.P., Tsegaye, G., Holt, G.T., Hu, A., Walpita, D., et al. (2016). Sensitive red protein calcium indicators for imaging neural activity. eLife *5*, e12727. https://doi.org/10.7554/eLife.12727.

37. Hao, Y.A., Lee, S., Roth, R.H., Natale, S., Gomez, L., Taxidis, J., O'Neill, P.S., Villette, V., Bradley, J., Wang, Z., et al. (2024). A fast and responsive voltage indicator with enhanced sensitivity for unitary synaptic events. Neuron *112*, 3680–3696.e8. https://doi.org/10.1016/j.neuron.2024.08.019.

38. Pak, V.V., Ezeriņa, D., Lyublinskaya, O.G., Pedre, B., Tyurin-Kuzmin, P.A., Mishina, N.M., Thauvin, M., Young, D., Wahni, K., Martínez Gache, S.A., et al. (2020). Ultrasensitive Genetically Encoded Indicator for Hydrogen Peroxide Identifies Roles for the Oxidant in Cell Migration and Mitochondrial Function. Cell Metab. *31*, 642–653.e6. https://doi.org/10.1016/j.cmet.2020.02.003.

39. Xiao, X., Yang, A., Zhang, H., Park, D., Wang, Y., Szabo, B., Boyden, E.S., and Piatkevich, K.D. (2025). Engineering of Genetically Encoded Bright Near-Infrared Fluorescent Voltage Indicator. Int. J. Mol. Sci. *26*, 1442. https://doi.org/10.3390/ijms26041442.

40. Inada, S., Hancox, J.C., Zhang, H., and Boyett, M.R. (2009). One-Dimensional Mathematical Model of the Atrioventricular Node Including Atrio-Nodal, Nodal, and Nodal-His Cells. Biophys. J. *97*, 2117–2127. https://doi.org/10.1016/j.bpj.2009.06.056.

41. Y. Yoshida, ed. (2021). Pluripotent Stem-Cell Derived Cardiomyocytes (Springer US). https://doi.org/10.1007/978-1-0716-1484-6.

42. Varghese, K., Das, M., Bhargava, N., Stancescu, M., Molnar, P., Kindy, M.S., and Hickman, J.J. (2009). Regeneration and characterization of adult mouse hippocampal neurons in a defined in vitro system. J. Neurosci. Methods *177*, 51–59. https://doi.org/10.1016/j.jneumeth.2008.09.022.

43. Kaestner, L., Scholz, A., Tian, Q., Ruppenthal, S., Tabellion, W., Wiesen, K., Katus, H.A., Müller, O.J., Kotlikoff, M.I., and Lipp, P. (2014). Genetically Encoded Ca^{2+} Indicators in Cardiac Myocytes. Circ. Res. *114*, 1623–1639. https://doi.org/10.1161/CIRCRESAHA.114.303475.

44. Shinnawi, R., Huber, I., Maizels, L., Shaheen, N., Gepstein, A., Arbel, G., Tijsen, A.J., and Gepstein, L. (2015). Monitoring Human-Induced Pluripotent Stem Cell-Derived Cardiomyocytes with Genetically Encoded Calcium and Voltage Fluorescent Reporters. Stem Cell Rep. *5*, 582–596. https://doi.org/10.1016/j.stemcr.2015.08.009.

45. Pioner, J.M., Santini, L., Palandri, C., Langione, M., Grandinetti, B., Querceto, S., Martella, D., Mazzantini, C., Scellini, B., Giammarino, L., et al. (2022). Calcium handling maturation and adaptation to increased substrate stiffness in human iPSC-derived cardiomyocytes: The impact of full-length dystrophin deficiency. Front. Physiol. *13*, 1030920. https://doi.org/10.3389/fphys.2022.1030920.

46. Djemai, M., Cupelli, M., Boutjdir, M., and Chahine, M. (2023). Optical Mapping of Cardiomyocytes in Monolayer Derived from Induced Pluripotent Stem Cells. Cells *12*, 2168. https://doi.org/10.3390/cells12172168.

47. Tian, L., Hires, S.A., Mao, T., Huber, D., Chiappe, M.E., Chalasani, S.H., Petreanu, L., Akerboom, J., McKinney, S.A., Schreiter, E.R., et al. (2009). Imaging neural activity in worms, flies and mice with improved GCaMP calcium indicators. Nat. Methods *6*, 875–881. https://doi.org/10.1038/nmeth.1398.

48. Quicke, P., Song, C., McKimm, E.J., Milosevic, M.M., Howe, C.L., Neil, M., Schultz, S.R., Antic, S.D., Foust, A.J., and Knöpfel, T. (2019). Single-Neuron Level One-Photon Voltage Imaging With Sparsely Targeted Genetically Encoded Voltage Indicators. Front. Cell. Neurosci. *13*, 39. https://doi.org/10.3389/fncel.2019.00039.

49. Yang, H., Stebbeds, W., Francis, J., Pointon, A., Obrezanova, O., Beattie, K.A., Clements, P., Harvey, J.S., Smith, G.F., and Bender, A. (2022). Deriving waveform parameters from calcium transients in human iPSC-derived cardiomyocytes to predict cardiac activity with machine learning. Stem Cell Rep. *17*, 556–568. https://doi.org/10.1016/j.stemcr.2022.01.009.

50. Roberts, R.J., and Lam, C.K. (2024). Application of Calcium Kinetics Characterization in Cardiac Disease Modeling and Drug Discovery. Biomolecules *14*, 865. https://doi.org/10.3390/biom14070865.

51. Seguret, M., Davidson, P., Robben, S., Jouve, C., Pereira, C., Lelong, Q., Deshayes, L., Cerveau, C., Le Berre, M., Rodrigues Ribeiro, R.S., and Hulot, J.S. (2024). A versatile high-throughput assay based on 3D ring-shaped cardiac tissues generated from human induced pluripotent stem cell derived cardiomyocytes. eLife *12*, RP87739. https://doi.org/10.7554/eLife.87739.2.

52. Ernst, P., Bidwell, P.A., Dora, M., Thomas, D.D., and Kamdar, F. (2022). Cardiac calcium regulation in human induced pluripotent stem cell cardiomyocytes: Implications for disease modeling and maturation. Front. Cell Dev. Biol. *10*, 986107. https://doi.org/10.3389/fcell.2022.986107.

53. Haridhasapavalan, K.K., Borgohain, M.P., Dey, C., Saha, B., Narayan, G., Kumar, S., and Thummer, R.P. (2019). An insight into non-integrative gene delivery approaches to generate transgene-free induced pluripotent stem cells. Gene *686*, 146–159. https://doi.org/10.1016/j.gene.2018.11.069.

54. Vargas, J.E., Chicaybam, L., Stein, R.T., Tanuri, A., Delgado-Cañedo, A., and Bonamino, M.H. (2016). Retroviral vectors and transposons for stable gene therapy: advances, current challenges and perspectives. J. Transl. Med. *14*, 288. https://doi.org/10.1186/s12967-016-1047-x.

55. Hackett, P.B., Largaespada, D.A., Switzer, K.C., and Cooper, L.J.N. (2013). Evaluating risks of insertional mutagenesis by DNA transposons in gene therapy. Transl. Res. *161*, 265–283. https://doi.org/10.1016/j.trsl.2012.12.005.

56. Zhao, M., Tanourlouee, S.B., McCracken, S., and Williams, P.R. (2025). Genetically encoded biosensors of metabolic function for the study of neurodegeneration, a review and perspective. Neurophotonics *12*, S22805. https://doi.org/10.1117/1.NPh.12.S2.S22805.

57. Dolgin, E. (2023). Self-copying RNA vaccine wins first full approval: what's next? Nature *624*, 236–237. https://doi.org/10.1038/d41586-023-03859-w.

58. Tolomeo, A.M., Laterza, C., Grespan, E., Michielin, F., Canals, I., Kokaia, Z., Muraca, M., Gagliano, O., and Elvassore, N. (2021). NGN2 mmRNA-Based Transcriptional Programming in Microfluidic Guides hiPSCs Toward Neural Fate With Multiple Identities. Frontiers in Cellular Neuroscience *15*, 602888. https://doi.org/10.3389/fncel.2021.602888.

59. Lin, H.-C., Janssens, J., Eisinger, B., Hornauer, P., Kroell, A.-S., Santel, M., Pascual-Garcia, M., Okamoto, R., Karava, K., He, Z., et al. (2025). Human neuron subtype programming via single-cell transcriptome-coupled patterning screens. Science *389*, eadn6121. https://doi.org/10.1126/science.adn6121.

60. Lin, H.-C., He, Z., Ebert, S., Schörnig, M., Santel, M., Nikolova, M.T., Weigert, A., Hevers, W., Kasri, N.N., Taverna, E., et al. (2021). NGN2 induces diverse neuron types from human pluripotency. Stem Cell Rep. *16*, 2118–2127. https://doi.org/10.1016/j.stemcr.2021.07.006.

61. Limone, F., Guerra San Juan, I., Mitchell, J.M., Smith, J.L.M., Raghunathan, K., Meyer, D., Ghosh, S.D., Couto, A., Klim, J.R., Joseph, B.J.,

et al. (2023). Efficient generation of lower induced motor neurons by coupling Ngn2 expression with developmental cues. Cell Rep. *42*, 111896. https://doi.org/10.1016/j.celrep.2022.111896.

62. Ribeiro, A.J.S., Guth, B.D., Engwall, M., Eldridge, S., Foley, C.M., Guo, L., Gintant, G., Koerner, J., Parish, S.T., Pierson, J.B., et al. (2019). Considerations for an In Vitro, Cell-Based Testing Platform for Detection of Drug-Induced Inotropic Effects in Early Drug Development. Part 2: Designing and Fabricating Microsystems for Assaying Cardiac Contractility With Physiological Relevance Using Human iPSC-Cardiomyocytes. Front. Pharmacol. *10*, 934. https://doi.org/10.3389/fphar.2019.00934.
63. Zhang, H., Yamaguchi, T., Kokubu, Y., and Kawabata, K. (2022). Transient ETV2 Expression Promotes the Generation of Mature Endothelial Cells from Human Pluripotent. Stem Cell. *45*, 483–490. https://www.jstage.jst.go.jp/article/bpb/45/4/45_b21-00929/_article.
64. Gest, A.M.M., Sahan, A.Z., Zhong, Y., Lin, W., Mehta, S., and Zhang, J. (2024). Molecular Spies in Action: Genetically Encoded Fluorescent Biosensors Light up Cellular Signals. Chem. Rev. *124*, 12573–12660. https://doi.org/10.1021/acs.chemrev.4c00293.
65. Wagner, T.E., Becraft, J.R., Bodner, K., Teague, B., Zhang, X., Woo, A., Porter, E., Alburquerque, B., Dobosh, B., Andries, O., et al. (2018). Small-molecule-based regulation of RNA-delivered circuits in mammalian cells. Nat. Chem. Biol. *14*, 1043–1050. https://doi.org/10.1038/s41589-018-0146-9.
66. Yousefpour, P., Gregory, J.R., Si, K., Lonzaric, J., Li, Y., Wang, J., Qureshi, K., Ledbetter, A., Lemnios, A.A., Dye, J., et al. (2026). Engineering drug-responsive replication machinery for precise control of self-amplifying RNA. Nat. Biomed. Eng. https://doi.org/10.1038/s41551-026-01723-6.
67. Lim, T.K.Y., Ritoux, A., Paine, L.W., Ferguson, L., Abdul, T., Grundy, L.J., and Smith, E.S.J. (2025). Cap-independent co-expression of dsRNA-sensing and NF-κB pathway inhibitors enables controllable self-amplifying RNA expression with reduced immunotoxicity. eLife *14*, RP105978. https://doi.org/10.7554/eLife.105978.
68. Gu, Y., Choi, J., Mutha, D., Wu, C., Ganem, N.J., Grinstaff, M.W., and Wong, W.W. (2026). Self-amplifying RNA-based CAR T cell therapy with enhanced duration and multi-genic logic functions. Preprint at bioRxiv. https://doi.org/10.64898/2026.02.18.706661.
69. Gong, Y., Yong, D., Liu, G., Xu, J., Ding, J., and Jia, W. (2024). A Novel Self-Amplifying mRNA with Decreased Cytotoxicity and Enhanced Protein Expression by Macrodomain Mutations. Adv. Sci. *11*, 2402936. https://doi.org/10.1002/advs.202402936.
70. Saeedi Saravi, S.S., Eroglu, E., Waldeck-Weiermair, M., Sorrentino, A., Steinhorn, B., Belousov, V., and Michel, T. (2020). Differential endothelial signaling responses elicited by chemogenetic H2O2 synthesis. Redox Biol. *36*, 101605. https://doi.org/10.1016/j.redox.2020.101605.
71. Shen, Y., Wu, S.-Y., Rancic, V., Aggarwal, A., Qian, Y., Miyashita, S.-I., Ballanyi, K., Campbell, R.E., and Dong, M. (2019). Genetically encoded fluorescent indicators for imaging intracellular potassium ion concentration. Commun. Biol. *2*, 18. https://doi.org/10.1038/s42003-018-0269-2.
72. Wang, N.B., Adewumi, H.O., Lende-Dorn, B.A., Beitz, A.M., O'Shea, T.M., and Galloway, K.E. (2025). Compact transcription factor cassettes generate functional, engraftable motor neurons by direct conversion. Cell Syst. *16*, 101206. https://doi.org/10.1016/j.cels.2025.101206.
73. Stirling, D.R., Swain-Bowden, M.J., Lucas, A.M., Carpenter, A.E., Cimini, B.A., and Goodman, A. (2021). CellProfiler 4: improvements in speed, utility and usability. BMC Bioinf. *22*, 433. https://doi.org/10.1186/s12859-021-04344-9.
74. Lian, X., Hsiao, C., Wilson, G., Zhu, K., Hazeltine, L.B., Azarin, S.M., Raval, K.K., Zhang, J., Kamp, T.J., and Palecek, S.P. (2012). Robust cardiomyocyte differentiation from human pluripotent stem cells via temporal modulation of canonical Wnt signaling. Proc. Natl. Acad. Sci. USA *109*, E1848–E1857. https://doi.org/10.1073/pnas.1200250109.
75. Lian, X., Zhang, J., Azarin, S.M., Zhu, K., Hazeltine, L.B., Bao, X., Hsiao, C., Kamp, T.J., and Palecek, S.P. (2013). Directed cardiomyocyte differentiation from human pluripotent stem cells by modulating Wnt/β-catenin signaling under fully defined conditions. Nat. Protoc. *8*, 162–175. https://doi.org/10.1038/nprot.2012.150.
76. Klapoetke, N.C., Murata, Y., Kim, S.S., Pulver, S.R., Birdsey-Benson, A., Cho, Y.K., Morimoto, T.K., Chuong, A.S., Carpenter, E.J., Tian, Z., et al. (2014). Independent optical excitation of distinct neural populations. Nat. Methods *11*, 338–346. https://doi.org/10.1038/nmeth.2836.
77. Trepotec, Z., Geiger, J., Plank, C., Aneja, M.K., and Rudolph, C. (2019). Segmented poly(A) tails significantly reduce recombination of plasmid DNA without affecting mRNA translation efficiency or half-life. RNA *25*, 507–518. https://doi.org/10.1261/rna.069286.118.
78. Peterman, E.L., Ploessl, D.S., Love, K.S., Sanabria, V., Daniels, R.F., Johnstone, C.P., Godavarti, D.R., Kabaria, S.R., Oakes, C.G., Pai, A.A., and Galloway, K.E. (2025). High-resolution profiling reveals coupled transcriptional and translational regulation of transgenes. Nucleic Acids Res. *53*, gkaf528. https://doi.org/10.1093/nar/gkaf528.
79. Yang, E.J.-N., Boldogh, I.R., Ji, H., Pon, L., and Swayne, T.C. (2023). Imaging of mtHyPer7, a Ratiometric Biosensor for Mitochondrial Peroxide, in Living Yeast Cells. JoVE J. *196*, e65428. https://doi.org/10.3791/65428.
80. ThermoFisher Scientific Cardiomyocyte differentiation from PSC suspension culture. https://documents.thermofisher.com/TFS-Assets/BID/Reference-Materials/cardiomyocyte-differentiation-from-psc-suspension-culture-protocol.pdf

Please cite this article in press as: Della Santina et al., Self-amplifying RNA enables rapid, durable, integration-free programming of hiPSCs, Cell Reports Methods (2026), https://doi.org/10.1016/j.crmeth.2026.101602

STAR★METHODS

KEY RESOURCES TABLE

REAGENT or RESOURCE	SOURCE	IDENTIFIER
Antibodies		
mouse anti-TUBB3 (TUJ1)	Biolegend	Cat# 801202; RRID: AB_10063408
rabbit anti-MAP2	Cell Signaling Technology	Cat# #4542; RRID: AB_10693782
goat anti-mouse Alexa Fluor 555	Invitrogen	Cat# A-21422; RRID: AB_2535844
donkey anti-rabbit Alexa Fluor 647	Jackson ImmunoResearch Labs	Cat# 711–605-152; RRID: AB_2492288
anti-human SSEA-4 APC-Vio® 770, REAfinity™	Miltenyi Biotec	Cat# 130–125-975; RRID: AB_2876945
mouse anti-cTnT	Abcam	Cat# ab8295; RRID: AB_306445
rabbit anti-Nkx2.5	Cell Signaling Technology	Cat# 8792; RRID: AB_2797667
goat anti-mouse 594	Invitrogen	Cat# A11005; RRID: AB_2534073
chicken anti-rabbit 647	Invitrogen	Cat# A21443; RRID: AB_2535861
goat anti-OCT-3/4	Santa Cruz	Cat# sc-8628; RRID: AB_653551
rabbit anti-cleaved caspase-3	Abcam	Cat# ab32042; RRID: AB_725947
Rabbit anti-cTnT	ABclonal	Cat# A4914; RRID: AB_2863388
Bacterial and virus strains		
NEB® Stable Competent *E. coli*	New England Biolabs	Cat# C3040I
Chemicals, peptides, and recombinant proteins		
AscI	New England Biolabs	Cat# R0558S
MluI-HF®	New England Biolabs	Cat# R3198S
Sph-HF®	New England Biolabs	Cat# R3182S
XbaI	New England Biolabs	Cat# R0145S
PrimeSTAR® HS DNA Polymerase	Takara Bio	Cat# R040A
Agarose Dissolving Buffer	Zymo Research	Cat# D4001-1-100
Pyrophosphatase, Inorganic (*E. coli*)	New England Biolabs	Cat# M0361S
DNase I	New England Biolabs	Cat# M0303S
CleanCap® Reagent AU	TriLink Biotechnologies	Cat# *N*-7114–5
CleanCap® Reagent AG	TriLink Biotechnologies	Cat# *N*-7113–5
Puromycin	Invivogen	Cat# ant-pr-1
Puromycin, 10mg/mL in distilled water, sterile-filtered	Thermo Scientific	Cat# J67236.XF
Zeocin™	Invivogen	Cat# ant-zn-05
StemFlex™ Medium	ThermoFisher	Cat# A3349401
Lipofectamine™ Stem Transfection Reagent	ThermoFisher	Cat# STEM00015
Lipofectamine™ MessengerMAX™ Transfection Reagent	ThermoFisher	Cat# LMRNA008
RevitaCell™ Supplement	ThermoFisher	Cat# A2644501
Gentle Cell Dissociation Reagent™	STEMCELL Technologies	Cat# 100–1077
DAPI	Tocris	Cat# 5748
Recombinant Human BDNF Protein	R&D Systems	Cat# 248-BDB-050
Human NT-3 Recombinant Protein	PeproTech®	Cat# 450-03-10UG
Trypan Blue Stain 0.4%	Invitrogen	Cat# T10282
CellAdhere Laminin-521	STEMCELL Technologies	Cat# 200–0117
Opti-MEM™ I Reduced Serum Medium	Thermo Scientific	Cat# 31985070
Penicillin-Streptomycin (10,000 U/mL)	Thermo Scientific	Cat# 15–140-122

(*Continued on next page*)

Continued

REAGENT or RESOURCE	SOURCE	IDENTIFIER
MEM Non Essential Amino Acids Solution (100×)	Thermo Scientific	Cat# 11–140-050
GlutaMAX Supplement	Thermo Scientific	Cat# 35–050-061
DMEM/F-12, no glutamine	Thermo Scientific	Cat# 21–331-020
B-27 Supplement (50×), serum free	Thermo Scientific	Cat# 17–504-044
N-2 Supplement (100×)	Thermo Scientific	Cat# 17–502-048
Paraformaldehyde, 16% w/v aq. soln., methanol free	Thermo Scientific	Cat# 043368-9 M
Bovine Serum Albumin (BSA)	Sigma Aldrich	Cat# A2058-25G
Bovine Serum Albumin Solution	Millipore Sigma	Cat# A1595
Bovine Serum Albumin lyophilized powder	Sigma Aldrich	Cat# A2153-50G
Hoechst 33342	Thermo Scientific	Cat# 62249
RPMI 1640 Medium	Gibco	Cat# 11875093
DMEM/F12	Gibco	Cat# 11320033
StemScale™ PSC Suspension Medium	Gibco	Cat# A4965001
Matrigel® Matrix hESC-qualified	Corning	Cat# 354277
StemPro™ Accutase®	Gibco	Cat# 11105–01
TrypLE Express™	Gibco	Cat# 12604–013
Y-27632 (Dihydrochloride)	STEMCELL Technologies	Cat# 72304
InSolution™ Y-27632, Sterile-Filtered, Cell Culture Tested	Millipore Sigma	Cat# 509228
Laduviglusib (CHIR-99021) HCl	Selleck Chemicals	Cat# S2924
IWP 2	Fisher Scientific	Cat# 35–331-0
CloneR™ 2	STEMCELL Technologies	Cat# 100–0691
mTeSR Plus medium	STEMCELL Technologies	Cat# 100–0276
RPMI 1640 [-] glucose	Thermo Scientific	Cat# 11879020
L-ascorbic acid 2-phosphate	Sigma-Aldrich	Cat# TA9H9876E755
Human Albumin	Sigma Aldrich	Cat# A9731
sodium L-lactate	Sigma Aldrich	71718
Triton X-100	Millipore Sigma	Cat# 1.08603.1000
B-27™ Supplement, minus insulin	Thermo Fisher Scientific	Cat# A1895601
ReLeSR™	STEMCELL Technologies	Cat# 100–0483
JumpStartTM Taq DNA Polymerase	Sigma-Aldrich	Cat# D9307-50UN
(±) -Propranolol hydrochloride	Millipore Sigma	Cat# P0884
(−) -Isoproterenol hydrochloride	Millipore Sigma	Cat# I6504
Papain	Worthington Biochem	Cat# 9001–73-4
Ovomucoid trypsin inhibitor	Worthington Biochem	Cat# 9035–81-1
Minimum Essential Medium (MEM, no glutamine, no phenol red)	Gibco	Cat# 51200038
D-glucose	Sigma	Cat# G7021
Holo-Transferrin bovine	Sigma	Cat# T0665
HEPES	Sigma	Cat# H0887
glutaGRO	Corning	Cat# 25–015-CI
insulin	Sigma	Cat# I9278
Heat-inactivated fetal bovine serum	Corning	Cat# 35–011-CV
AraC	Sigma	Cat# C6645
Pluronic™ F-127	Invitrogen	Cat# P6866
RPMI 1640 Medium, no phenol red	Gibco	Cat# 11835030

(*Continued on next page*)

Continued

REAGENT or RESOURCE	SOURCE	IDENTIFIER
Critical commercial assays		
LIVE/DEAD™ Fixable Orange (602) Viability Kit	Thermo Scientific	Cat# L34984
NEBuilder® HiFi DNA Assembly Cloning Kit	New England Biolabs	Cat# E5520S
HiScribe® T7 High Yield RNA Synthesis Kit	N/A	Cat# E2040S
Monarch Total RNA Miniprep Kit	New England Biolabs	Cat# T2010
Protoscript First Strand cDNA synthesis Kit	New England Biolabs	Cat# E6300
Monarch® Spin RNA Cleanup Kit (50 μg)	New England Biolabs	Cat# T2040S
Monarch® Spin PCR & DNA Cleanup Kit (5 μg)	New England Biolabs	Cat# T1130L
Monarch® Spin Plasmid Miniprep Kit	New England Biolabs	Cat# T1110L
LookOut® Mycoplasma PCR Detection Kit	Millipore Sigma	Cat# MP0035-1KT
STEMdiff™ Cardiomyocyte Dissociation Kit	STEMCELL Technologies	Cat# 05025
Zymo 1× DNA/RNA Shield	Zymo	Cat# R110S
Fluo-4 AM, cell permeant	Invitrogen	Cat# F14201
CellROX™ Orange Reagent	Invitrogen	Cat# C10443
MitoView™ 633	Biotium	Cat# 70055
Calcein Blue, AM	ThermoFisher	Cat# C1429
Deposited data		
RNA Seq. of saRNA treated, modRNA treated, and control iPS11 at 24 and 48 h post transfection	Gene Expression Omnibus (GEO)	GSE334590
Experimental models: Cell lines		
Human: Human iPSC Line (Episomal, HFF)	Alstem	Cat# iPS11
Human: Human iPSC Line	UPenn Dr. Daniel Rader	PENN014i-37–3
Swiss Webster Mouse (hippocampus cell culture)	Taconic Biosciences	SW-F/SW-M
Oligonucleotides		
polyA-encoded. Sequence: GGATTTTGTTTTTAA TATTTCAAAAAAAAAAAAAAAAAAAAAAAAAA AAAAAAAAAAAAAAAAAAAAAAAAAAAAAA AAAAAGAAAAAAAAAAAAAAAAAAAAAAAA AAAAAAAAAAAAAAAAAAAAAAAAAAAAAA AAACGCGTCGAGGGGAATTAATTCTTGAAG	Integrated DNA Technologies	4 nmole Ultramer™ DNA Oligo
DP-369. Sequence: ggtgcctgagaattggcaag	Genewiz from Azenta Life Sciences	N/A
DP-370. Sequence: ttttttttgaaatattaa aaacaaaatcc	Genewiz from Azenta Life Sciences	N/A
qPCR primers, see Table S1	Genewiz from Azenta Life Sciences	N/A
Recombinant DNA		
pIVT-Flp-2A-BleoR	Blanch-Asensio et al.[32]	Addgene Plasmid #232752
pAAV.Syn.NES-jRCaMP1b.WPRE.SV40	Dana et al.[36]	Addgene Plasmid #100851
pAAV-hsyn-ASAP5-WPRE	Hao et al.[37]	Addgene Plasmid # 225709
HyPer7.2DAAO-mito	Saeedi Saravi et al.[70]	Addgene Plasmid #168304
pcDNA3.1-GINKO1	Shen et al.[71]	Addgene Plasmid #113112
pMXs-NIL	Wang et al.[72]	Addgene Plasmid # 233192
T7-VEE-GFP	Yoshioka et al.[16]	Addgene Plasmid #58977
pKG03372-VEE-eGFP-IRES-PuroR-polyA	This Study	Addgene Plasmid #246033
pKG04056-VEE-eGFP-IRES-BleoR-polyA	This Study	Addgene Plasmid # 246034
pKG03865-VEE-jRCaMP1b-IRES-PuroR-polyA	This Study	Addgene Plasmid # 246035
pKG03866-VEE-ASAP5-IRES-PuroR-polyA	This Study	Addgene Plasmid # 246036
pKG04057-VEE-HyPer7-IRES-PuroR-polyA	This Study	Addgene Plasmid # 246037

(*Continued on next page*)

Continued

REAGENT or RESOURCE	SOURCE	IDENTIFIER
pKG03863-VEE-Ngn2-P2A-eGFP-IRES-PuroR-polyA	This Study	Addgene Plasmid # 246038
pKG04063-pSHIP-CAG.d-eGFP-IRES-PuroR-bGH	This Study	Addgene Plasmid # 246040
pKG03869-pIVT-eGFP-IRES-PuroR-polyA	This Study	Addgene Plasmid # 246041
pKG04347-VEE-GINKO1-IRES-PuroR-polyA	This Study	Addgene Plasmid # 246057
Software and algorithms		
Fiji/ImageJ2	N/A	2.9.0/1.53t
MATLAB_R2023A	Mathworks	N/A
GraphPad Prism 8	GraphPad	v. 8.2.0
SnapGene®	SnapGene	N/A
Adobe Illustrator CC	N/A	https://www.adobe.com
FlowJo software	FlowJo	https://www.flowjo.com
CellProfiler 4.2.8	Stirling et al.[73]	Cellprofiler.org

EXPERIMENTAL MODEL AND STUDY PARTICIPANT DETAILS

All procedures involving animals at the Massachusetts Institute of Technology were conducted in accordance with the United States National Institutes of Health Guide for the Care and Use of Laboratory Animals and approved by the Massachusetts Institute of Technology Committee on Animal Care and Biosafety Committee.

iPS11 cells (Alstem, iPS11) were maintained on 24-well plates coated with 15 μL CellAdhere Laminin-521 (STEMCELL Technologies, 200–011), media changed daily with 500 μL Gibco Stemflex (ThermoFisher Scientific, A3349401) containing 100 U/mL Penicillin-Streptomycin (ThermoFIsher Scientific, 15140122) and incubated in a humidified incubator at 37°C with 5% CO_2. Cells were passaged at a split ratio of 1:10 twice a week when ~80% confluent using 300 μL Gentle Cell Dissociation Reagent (STEMCELL Technologies, 100–1077) according to the manufacturer's instructions and replated with 1:200 RevitaCell Supplement (ThermoFisher Scientific, A2644501). iPS11 are used in Figures 1B–1F and 2B–2G.

37–1189 cells (generously provided by University of Pennsylvania under MTA agreement, PENN0141-37-3) were maintained on 6-well plates coated with hESC qualified Matrigel (Corning, 354277) diluted in 500 mL DMEM/F12 media (Gibco, 11320033), media changed every other day with 2 mL Gibco Stemflex (ThermoFisher Scientific, A3349401) and incubated in a humidified incubator at 37°C with 5% CO_2. Cells were passaged at a split ratio between 1:3 and 1:6 when <60% confluent using 1 mL ReLeSR™ (STEMCELL Technologies, 100–0483) according to manufacturer's instructions. 37–1189 cells are used in Figures 1G and 1H and 4B–4I.

hiPSC-derived CMs were obtained by differentiation of 37–1189 hiPSCs.[74,75] hiPSCs were maintained on Matrigel-coated plates (Corning, 354277) in mTeSR Plus medium (STEMCELL Technologies, 100–0276), with medium changes every two days. Cells were passaged using ReLeSR (STEMCELL Technologies, 100–0483) according to manufacturer instructions. For differentiation, cells were seeded onto Matrigel (Corning, 354277) in a 12-well plate at a concentration of 100,000 cells per well, allowed to grow for 3 days, and then treated with 12 μM CHIR-99021 (Selleck Chemicals, S2924) for 24 h in RPMI 1640 (ThermoFisher Scientific, 11875093) with B27 supplement, minus insulin (ThermoFisher Scientific, A1895601). Exactly 48 h after removal of CHIR-99021, the cells were treated with 5 μM of the Wnt inhibitor IWP-2 (Fisher Scientific, 35–331-0) and incubated for another 48 h. RPMI/B27 minusinsulin media was changed every other day for 7 days after the addition of CHIR-99021, following 7 days of culture in RPMI/B27 minus insulin, the media was changed to RPMI with B27 supplement, serum-free (ThermoFisher Scientific, 17504044). To select for cardiomyocytes, cells were cultured for 3 days in RPMI 1640 without glucose (ThermoFisher Scientific, 11879020) supplemented with 213 μg/mL L-ascorbic acid 2-phosphate (Sigma-Aldrich, TA9H9876E755), 500 μg/mL human albumin (Sigma Aldrich, A9731), and 5 mM sodium L-lactate (Sigma Aldrich, 71718). Cardiomyocytes were replated using the STEMdiff Cardiomyocyte Dissociation Kit (StemCell Technologies 05025) and plated onto a Matrigel-coated plate for imaging at day 14. hiPSC CMs were used in Figures 3B and 3D.

Primary mouse hippocampal explant cultures were prepared from postnatal day 0 or 1 Swiss Webster mice (Taconic) (both male and female mice were used) as previously described (Klapoetke et al., 2014[76]). Briefly, dissected hippocampal tissue was digested with 100 units of papain (Worthington Biochem) for 6–8 min, and the digestion was stopped with ovomucoid trypsin inhibitor (Worthington Biochem). Cells were seeded in 100 μL neuron culture medium containing Minimum Essential Medium (MEM, no glutamine, no phenol red; Gibco), D-glucose (25 mM, Sigma), holo-Transferrin bovine (100 μg/mL, Sigma), HEPES (10 mM, Sigma), glutaGRO (2 mM, Corning), insulin (25 μg/mL, Sigma), B27 supplement (1×, Gibco), and heat-inactivated fetal bovine serum (10% in volume, Corning), with final pH adjusted to 7.3–7.4 using NaOH. After cell adhesion, additional plating medium was added. AraC (2 μM, Sigma) medium was added at 1 day *in vitro* (DIV 1), when glial density was 50%–70% of confluence. Neurons were grown at 37°C and 5% CO2 in a humidified atmosphere in a neuron incubator, with 2 mL total medium volume in each well of the 24-well plate. Primary mouse hippocampal explant cultures are used in Figures 3C and 3E.

Please cite this article in press as: Della Santina et al., Self-amplifying RNA enables rapid, durable, integration-free programming of hiPSCs, Cell Reports Methods (2026), https://doi.org/10.1016/j.crmeth.2026.101602

METHOD DETAILS

Molecular cloning

All self-amplifying RNA IVT templates were derived from T7-VEE-GFP (Addgene Plasmid #58977). To streamline saRNA production, T7-VEE-eGFP-IRES-PuroR-polyA (Addgene Plasmid #246033), which encodes a polyA track downstream of the 3′ conserved sequence element was constructed. This enables T7 RNA polymerase to append a polyA tail on transcribed saRNAs within the IVT reaction, eliminating the need to carry out an additional polyadenylation reaction required for saRNAs derived from the original vector. To achieve this, a 4 nmol DNA ultramer oligo (Integrated DNA Technologies), polyA-encoded, which contained a segmented polyA ($poly(A)_{2 \times 60\_G}$) previously reported to attenuate *in vivo* truncation in E. coli[77] flanked with Gibson overhangs was ordered. T7-VEE GFP was digested with Sph-HF and MluI-HF, which correspond to the unique restriction sites closest to the desired placement of a polyA track. As the digestion of T7-VEE GFP with Sph-HF excised the C-terminus of PuroR and the 3′ conserved sequence element, the corresponding sequence from T7-VEE GFP was PCR amplified with primers DP-369 and DP-370. These and all subsequent digested vectors and PCR-generated DNA fragments were isolated via gel electrophoresis, extracted with Agarose Dissolving Buffer (Zymo Research, D4001-1-100), and purified with the Monarch PCR and DNA Cleanup Kit (NEB). 40 ng of digested backbone, 40 ng PCR product, and 4 ng of polyA-encoded oligo were assembled using HiFi reaction mixture (NEB). The reaction was transformed to NEB Stable bacteria and incubated overnight on LB + Ampicillin Agar plates. Individual colonies were cultured in 5 mL liquid LB + Ampicillin, with overnight cultures miniprepped using the Monarch miniprep kit. All incubation steps were conducted at 30°C to minimize truncation of the polyA track.

All saRNA IVT templates were assembled via HiFi assembly following an analogous procedure. The eGFP-IRES-PuroR cassette from T7-VEE-eGFP-IRES-PuroR-polyA was excised by digestion with AscI and XbaI. The digested backbone was treated with shrimp alkaline phosphatase to attenuate background colonies. Genes of interest were PCR amplified with 20–30 bp long Gibson-compatible overhangs with PrimeSTAR HS DNA Polymerase (Takara). BleoR was cloned from pIVT-Flp-2A-BleoR (Addgene Plasmid #232752), jRCaMP1b was cloned from pAAV.Syn.NES-jRCaMP1b.WPRE.SV40 (Addgene Plasmid #100851), ASAP5 was cloned from pAAV-hsyn-ASAP5-WPRE (Addgene Plasmid # 225709), HyPer7 was cloned from HyPer7.2DAAO-mito (Addgene Plasmid #168304), GINKO1 was cloned from pcDNA3.1-GINKO1 (Addgene Plasmid #113112) and Ngn2-P2A was cloned from pMXs-NIL (Addgene Plasmid # 233192).

The template for eGFP-IRES-PuroR modRNA, pIVT-eGFP-IRES-PuroR-polyA (Addgene Plasmid #246041) and eGFP-IRES-PuroR plasmid DNA expression vector, pSHIP-CAG.d-eGFP-IRES-PuroR-bGH (Addgene Plasmid #246040) were both constructed via BsaI Golden Gate following the Galloway Lab's version of MoClo, as previously reported.[78] Briefly, the eGFP-IRES-PuroR cassette was PCR amplified with compatible pPV2 BsaI overhangs. For pIVT-eGFP-IRES-PuroR-polyA, the PCR fragment was assembled into a modRNA IVT backbone plasmid containing beta globin 5′ and 3′ UTRs and a T7 promoter compatible with the CleanCap AG reagent. For pSHIP-CAG.d-eGFP-IRES-PuroR-bGH, the PCR fragment was assembled into a transcriptional unit containing a domesticated CAG promoter (CAG.d) and the bovine growth hormone (bGH) polyadenylation signal. Golden gate reactions were transformed as described above, substituting Ampicillin with Kanamycin.

All plasmids were sequence verified with Plasmidsaurus Whole Plasmid Sequencing and will be made available on Addgene.

In vitro transcription

Plasmids encoding the desired saRNAs were linearized for IVT with MluI-HF (New England Biolabs, R3198S) and purified using the Monarch PCR and DNA Cleanup Kit (New England Biolabs, T1030). 500 ng of purified linearized product served as template in a 20 μL IVT reaction using the HiScribe T7 High Yield RNA Synthesis Kit (New England Biolabs, E2040), co-transcriptionally capping with CleanCap Reagent AU (TriLink Biotechnologies, *N*-7114–1) for saRNA or CleanCap Reagent AG (TriLink Biotechnologies, *N*-7113–5) for modRNA. 1 μL of Pyrophosphatase, Inorganic (E. coli) (New England Biolabs, M0361S) was added to each IVT to enhance yield. IVT reactions were incubated at 37°C for 6 h, at which point reactions were diluted to 50 μL, treated with 2 μL DNase I (New England Biolabs, M0303), and incubated at 37°C for 30 min to degrade the IVT template DNA. Synthesized saRNA was column purified and eluted with 60 μL water using the 50 μg Monarch RNA Cleanup Kit (New England Biolabs, T2040). A small sample was nanodropped and run on a native denaturing gel to determine saRNA concentration and verify full-length product. The saRNA was dispensed in aliquots and stored at −80°C.

Transfection of hiPSCs with saRNA

Transfection experiments were conducted as described elsewhere.[32] Briefly, hiPSCs were plated the day prior at 100,000 cells per 24-well to achieve ~30% confluency on the day of transfection. 500 ng of saRNA was diluted in Opti-MEM (ThermoFisher Scientific, 31985070) to a volume of 25 μL. In parallel, either 1 μL of Lipofectamine Stem Transfection Reagent (ThermoFisher Scientific, STEM00015; for Figure 1 comparisons of plasmid DNA, modRNA, and saRNA) or 1 μL of Lipofectamine MessengerMAX Transfection Reagent (ThermoFisher Scientific, LMRNA008; for all other experiments involving exclusively modRNA and/or saRNA) was added to 24 μL Opti-MEM. For the Stem Transfection Reagent, the diluted saRNA was added immediately to the Lipofectamine mixture, mixed well, and incubated for 10 min. For the MessengerMax Transfection Reagent, the Lipofectamine mixture was preincubated for 15 min before adding the diluted saRNA, and the saRNA/Lipofectamine mixture was incubated for an additional 5 min. During the incubation periods, cells were optionally washed once with PBS, and media was replaced with 500 μL of Opti-MEM. After the final incubation

step, the saRNA/LNP complexes were added dropwise to the well, and the plate was gently rocked and returned to the incubator. After 4 h, 500 μL of StemFlex media was added to each transfected well. A complete media change was performed on transfected wells the following day.

QUANTIFICATION OF TRANSFECTION EFFICIENCY, CELL VIABILITY, AND PLURIPOTENCY MARKERS

iPS11 cells were transfected as above with 500 ng of either pDNA, modRNA, saRNA using Lipofectamine Stem Transfection Reagent. Two days post-transfection, cells were either fixed and stained for OCT4 or dissociated with TrypLE Express™ for flow cytometry assessment of viability and SSEA-4 staining.

For OCT4 staining, cells were PBS washed three times and fixed for 1 h at 4°C with Paraformaldehyde, 16% w/v aq. soln., methanol free (ThermoFisher Scientific, 043368-9 M) diluted to 4% in PBS. Cells were washed three times with PBS following fixation and blocking was performed in 2% BSA (Sigma-Aldrich, A2153-50G) with 0.1% Triton X-100 (Millipore Sigma, 1.08603.1000) for 1 h at room temperature. Primary antibody (goat anti-OCT-3/4, Santa Cruz sc-8628) was diluted 1:2500 in blocking buffer and 500 μL was added to each well overnight at 4°C. Primary antibody was removed, and cells were washed three times with PBS. Secondary antibody (chicken anti-goat Alexa 647, Invitrogen A-21469) was diluted 1:1000 in blocking buffer and incubated overnight at 4°C. Cells were then washed three times with PBS and incubated with 300 μL per well of Hoechst 33342 (Thermo Scientific, 62249) diluted 1:5000 in PBS for 5–10 min at room temperature. Cells were washed once with PBS then stored at 4°C protected from light and evaporation until ready to image. OCT4 nuclear intensity was quantified using Fiji. Briefly, single slice confocal images were taken at the center of the sample using a 20×0.7 NA objective (Nikon MRH48250). Once loaded into Fiji, individual color channels were split, and a threshold was imposed on the Hoechst channel using an Otsu range of 130–65535. These settings were used to convert the Hoechst channel to a Binary mask which was then adjusted with the 'fill holes' command and individual nuclei separated from each other with the 'watershed' command (both of which can be found in the Process > Binary dropdown menu). After visual inspection to assess accuracy of the mask, 'Analyze Particles' was run with size range set to 25–500 pixels (to remove small debris or ineffectively segmented nuclei from analysis) and 0–1 circularity. This mask was then applied to the OCT4 channel and the average measurement for each segmented nucleus was calculated to report across groups. Additional representative images were captured using an epifluorescence microscope (EVOS M5000 Imaging system); with 4×/10× phase ring, DAPI, Cy5, and 10× Objective, fluorite, LWD, phase-contrast, 0.30NA/7.13WD (Thermo Fisher, AMEP498).

For flow cytometry assessment, cell suspension was spun down at 300 g for 4 min and resuspended in 1mL PBS for staining with 1 μL LIVE/DEAD™ Fixable Orange (602) Viability Kit for 30 min at room temperature. The cells were pelleted, washed once with PBS, and then resuspended in 98 μL of PBS with 5% BSA (Millipore Sigma, A1595). The samples were then stained with 2 μL of Anti-human SSEA-4 APC-Vio 770, REAfinity (Miltenyi Biotec) and incubated in the dark for 15 min at 4°C. Cell suspensions were then diluted in 1 mL of cold PBS and pelleted for 10 min at 400 g and 4°C, resuspended in PBS, filtered and analyzed by flow cytometry.

Flow cytometry

Flow cytometry experiments were conducted on an Attune NxT Acoustic Focusing Cytometer using a 488 nm laser, 510/10 filter, and a voltage gain of 240 for eGFP fluorescence, a nm laser, 620/15 filter and a voltage gain of 400 for mOrange live/dead fluorescence, and a nm laser, 780/60 filter and a voltage gain of 400 for SSEA-4-APC-Vio7 fluorescence. FSC-A and SSC-A were used to gate cells, with FSC-H and FSC-A used to gate singlets. $eGFP^+$, mOrange live/$dead^-$, and SSEA-4-APC-$Vio7^+$ gates were set using an untransfected and unstained negative control sample. Gating and analysis were conducted using FlowJo. The gating strategy and representative histogram plots are presented in Figure S1. Raw.fcs are available on GitHub.

RNA sequencing and analysis

iPS11 cells were cultured in StemFlex (ThermoFisher, A3349401) media on Matrigel coated 6-well plates. Prior to transfection cells were dissociated using TrypLE express (Gibco, 12604–013) and seeded into a Matrigel (Corning, 354277) coated 24 well plate and allowed to adhere overnight. On day 0, cells were transfected with 250 ng of saRNA, modRNA, or no nucleic acid complexed with 0.5 μL Lipofectamine MessengerMax (ThermoFisher, LMRNA008) and Opti-MEM to a total volume of 25 μL per well. Each well was transfected in 250 μL of Opti-MEM per well for 4 h then 250 μL of StemFlex media was added to media contents and incubated overnight. On day 1 post transfection, wells were either media changed to be kept until day 2 or collected for sequencing. Briefly, wells were washed twice with PBS and incubated with 100 μL TrypLE express for 3–5 min at 37°C. Cells were gently pipetted up and down to singularize then were transferred to Eppendorf tubes with 400 μL StemFlex to neutralize dissociation. Cells were counted then centrifuged at 300 × g for 5 min and supernatant was removed. Cell pellets were then resuspended in, at minimum, 50 μL Zymo 1× DNA/RNA Shield (Zymo, R1100S) (use the appropriate volume to achieve ~200 K cells per 50 μL end volume), mixed immediately and thoroughly, then vortexed for 5 s to shear chromosomal DNA. Samples were stored at room temperature until submitting to Plasmidsaurus for RNA Sequencing. On day 2, all remaining wells were processed.

Quality of the fastq files was assessed using FastQC v0.12.1. Reads were then quality filtered using fastp v0.24.0 with poly-X tail trimming, 3′ quality-based tail trimming, a minimum Phred quality score of 15, and a minimum length requirement of 50 bp. Quality-filtered reads were aligned to the reference genome using STAR aligner v2.7.11 with non-canonical splice junction removal and output of unmapped reads, followed by coordinate sorting using samtools v1.22.1. PCR and optical duplicates were removed using

UMI-based deduplication with UMIcollapsev1.1.0. Alignment quality metrics, strand specificity, and read distribution across genomic features were assessed using RSeQC v5.0.4 and Qualimap v2.3, with results aggregated into a comprehensive quality control report using MultiQC v1.32. Gene-level expression quantification was performed using featureCounts(subread package v2.1.1) with strand-specific counting, multi-mapping read fractional assignment, exons and three prime UTR as the feature identifiers, and grouped by gene_id. Final gene counts were annotated with gene biotype and other metadata extracted from the reference GTF file.

hiPSC suspension spheroid culture

hiPSCs (37–1189) were seeded onto Matrigel (Corning, 354277) in DMEM/F12 (Gibco, 11320033) coated 24-well plate transfected as described above and maintained in 1 μg/mL puromycin (Thermo Scientific, J67236.XF) in StemFlex Media (ThermoFisher, A3349401) for 5 to 7 days depending on growth rate and required cell number. To seed into suspension, cells were washed twice with D-PBS and incubated with Stempro™ Accutase™ (ThermoFisher Scientific, A1110501) for 3–5 min at 37°C. Dissociated cells were gently triturated to singularize and added to a StemScale media volume that is 4 times that of Accutase to neutralize dissociation. Cell suspension was then centrifuged at 200 g for 4 min to pellet cells. Supernatant was aspirated and cell pellet was resuspended in StemScale™ PSC Suspension Medium (ThermoFisher Scientific, A4965001) media supplemented with Y-27632 (Millipore Sigma, 5092280001 or StemCell Technologies, 72304) to a final concentration of 10 μM. Live cells were counted using a Countess 3 (Invitrogen) cell counter with Trypan Blue Stain (Invitrogen, T10282) and added to a non-tissue culture treated 6 well plate at 300,000 cells per well in StemScale media with 10 μM Y-27632. Plates were then incubated on an orbital shaker (Thermo MaxQ 2000 CO_2 Plus) rotating at 70 rpm. Half media changes with StemScale were performed the day after seeding and every other day following by tilting the plate at a 45° angle, allowing the spheroids to settle, and gently aspirating and replacing half the media. Puromycin selection was withdrawn for seeding and optionally added back the day following seeding using a complete media change also performed by tilting the plate to a 45° angle and pipetting off and replacing the entire media volume.

Fixation, immunofluorescent staining, and purity quantification of induced neurons (iNs)

For induced neurons, immunostaining was carried out at 24-well scale at 6 dpt of Ngn2-P2A-eGFP. All wash/addition steps were carried out via manual aspiration (i.e., slowly removing or adding media with a P200 pipette), rotating the quadrant the pipette tip was submerged clockwise for each pipetting step to avoid over pipetting in one area of the well. Culture media was removed from iNs and cells were washed three times with PBS. Cells were fixed with 4% paraformaldehyde for 1 h at 4°C. After 1 h, the fixative was removed, and cells were washed three times with cold PBS. Cells were then blocked and permeabilized with 5% FBS and 0.5% Tween 20 in PBS for 24 h at 4°C. Following permeabilization and blocking, primary antibodies, either mouse anti-TUJ1 (BioLegend 801202) or rabbit anti-MAP2 (Cell Signaling Technologies 4542) were added at a 1:500 dilution in blocking buffer (5% FBS, 0.1% Tween 20 in PBS) and incubated overnight at 4°C. Cells were washed three times with 0.1% Tween 20 in PBS and blocked and permeabilized in 5% FBS and 0.5% Tween 20 in PBS for 1 h at 4°C. DAPI (1×) (Tocris 5748) and secondary antibodies, either goat anti-mouse Alexa Fluor 555 (Invitrogen, A-21422) or donkey anti-rabbit Alexa Fluor 647 (Jackson ImmunoResearch Laboratories, 711–605-152) were added at a 1:500 dilution in blocking buffer and incubated at room temperature for 1 h. Cells were washed with 0.1% Tween 20 in PBS three times and cells were kept in PBS following the last wash. Images and visualization were carried out with the Keyence All-in-one fluorescence microscope BZ-X800.

To quantify the purity of the induced neurons, five sections of a DAPI and TUJ1-stained well were randomly sampled and imaged. DAPI stained nuclei were segmented with CellProfiler,[73] using the IdentifyPrimaryObjects module. This module set the object diameter to a minimum of 8 pixels and a maximum of 50 pixels, implemented an adaptive Minimum Cross-Entropy thresholding method with a smoothing scale and correction factor of 1.65 and 1, respectively, and used pixel intensity to distinguish clumped objects. The pipeline is provided in a .zip folder on GitHub. After segmentation to obtain the total number of nuclei in the image section, the number of TUJ1-negative nuclei (corresponding to residual stem cells) were manually counted and subtracted from the total nuclei count to determine the number of TUJ1-positive nuclei (corresponding to the number of iNs). TUJ1-positive nuclei and total nuclei across all five image sections were summed and purity was calculated using the ratio of TUJ1-positive nuclei to total nuclei. An example of the segmentation strategy for one technical replicate is provided in Figure S5.

Quantitative PCR analysis of induced neurons (iNs)

Three separate differentiation experiments were conducted using iPS11. For each replicate, induced neurons obtained from three 24-wells transfected with Ngn2-2 A-eGFP saRNA and negative control cells obtained from one 24-well transfected with eGFP saRNA were harvested six days post transfection, resuspended in 200 μL of RNA later buffer, and stored at −80°C. RNA from all three experiments was isolated simultaneously using the Monarch Total RNA Miniprep Kit (New England Biolabs, T2010) with an additional on-column Dnase I (New England Biolabs, M0570) treatment step. RNA samples were eluted with 50 μL of nuclease-free water. cDNA was synthesized from 6 μL of eluted RNA using the ProtoScript First Strand cDNA Synthesis Kit (New England Biolabs, E6300) using oligo-dT primers. cDNA samples were stored at −20°C until qPCR.

qPCR was performed at the MIT BioMicro Center on a Roche LightCycler 480 with three technical replicates per condition. Reaction mixes were assembled using 5.0 μL KAPA SYBR FAST qPCR Master Mix (2×) Universal (Kapa Biosystems, KK4600), 0.5 μL 2 μM forward and reverse primers, 0.5 μL cDNA product, and 1.5 μL nuclease-free water. The primer sequences used for each gene target are provided in the supplemental information. Using the "High Sensitivity" analysis mode, C_t values were called for each technical

replicate, with average C_t values determined by calculating the arithmetic mean of the three technical replicates. $2^{-\Delta Ct}$ values were calculated relative to the RPL37A levels for each sample and $\log_{10}$ transformed.

Imaging of HyPer7 reporter

Generation of the HyPer7-Mito saRNA and transfection into hiPSCs was performed as described above. Two days post transfection, MitoTracker Deep Red FM dye (Thermo Fisher Scientific, M22426) was added to the cells at a concentration of 50nM and incubated at 37°C for 15 min. Culture medium was replaced with 1.2 mL of HBSS solution (Thermo Fisher Scientific, 14025092) supplemented with 20 mM HEPES (Thermo Fisher Scientific, 15630080). D-alanine (TCI, A0177) or Hydrogen Peroxide (H_20_2) (Thermo Fisher Scientific, H325-500) were added to the appropriate conditions to a final concentration of 40 mM and 25 μM, respectively. Imaging was performed using an Inverted Evident FluoView FV4000 microscope with a 60×/1.30 silicon immersion UPlan Superapochromat objective. The HyPer7 fluorophore was excited sequentially with 405 nm and 488 nm lasers, and emission was detected with a 520 nm filter. The HyPer7 ratio was calculated using the Fiji distribution of ImageJ by performing background subtraction, then dividing the mean intensity of each 488 nm excitation image (oxidized HyPer7) by the corresponding 405 nm excitation image (reduced HyPer7). Colorized ratio images were generated as previously described.[38,79] Briefly, each 488 nm excitation image was divided by its corresponding 405 nm excitation image, and the resulting image was depicted in the ''Fire'' lookup table.

Voltage and calcium imaging and analysis in 2D cell culture

Mouse hippocampal cell cultures were prepared at 24-well scale as described above and were transfected with 500 ng of saRNA diluted in Opti-MEM (ThermoFisher Scientific, 31985070) to a volume of 25 μL. In parallel, 1 μL of Lipofectamine MessengerMAX Transfection Reagent (ThermoFisher Scientific, LMRNA008) was added to 24 μL Opti-MEM. The Lipofectamine mixture was preincubated for 15 min before adding the diluted saRNA, and the saRNA/Lipofectamine mixture was incubated for an additional 5 min. After the final incubation step, the saRNA/LNP complexes were added dropwise to the well in 500 μL of maintenance media, and the plate was gently rocked and returned to the incubator. After 4 h, 500 μL of additional maintenance media was added to each transfected well. hiPSC-derived CMs were prepared at 96-well scale and were transfected with 100 ng saRNA in 5 μL Opti-MEM™ complexed with 0.2 μL Lipofectamine MessengerMAX Transfection Reagent in 4.8 μL Opti-MEM™ in 100 μL maintenance media and refreshed with an additional 100 μL of maintenance media after 4 h. A complete media change was performed on transfected wells the following day. Neural cultures were transfected at ≥ 14 days *in vitro* and hiPSC-derived cardiomyocytes were transfected once beating resumed following replating at day 14 (between 4 and 5 days).

Live neuron and cardiomyocyte imaging was performed in their maintenance media at room temperature on a spinning disk confocal microscope (a Yokogawa CSU-W1 Confocal Scanner Unit on a Nikon Eclipse Ti microscope) equipped with a 40×1.15 NA water immersion objective (Nikon MRD77410) and a Zyla PLUS 4.2 Megapixel camera controlled by NIS-Elements AR software. The filter set for GFP (488 nm excitation; FITC emission filter) was used for imaging ASAP5 and the filter set for mRuby (561 nm excitation; Cy3 emission) was used for imaging jRCaMP1b. Voltage imaging (ASAP5) was performed at 300 ms exposure (3.33 Hz) for neuronal cell types and 100 ms exposure (10 Hz) for cardiac cell types. Calcium imaging (jRCaMP1b) was performed at 100 ms exposure (10 Hz) for neuronal cell types and 100 ms exposure (10 Hz) for cardiac cell types. For each sample, imaging was performed on a single focal plane near the mid-section of cells. hiPSC-derived CMs with beating patterns that kept the cell body in focus were selected for representative traces. From primary mouse hippocampus cultures, cells with characteristic neuronal morphology, including small cell bodies and long, branched processes, were visually identified and treated as putative neurons. Sliding window normalization was applied to correct for slow baseline signal drift. Briefly, for each recorded trace, the raw fluorescence intensity vector was extracted, and a baseline fluorescence (F_0) was estimated using a sliding window set between 15 and 100. Within each window, the baseline was defined between the 10^{th} and 50^{th} percentile (median) of fluorescence values, providing an estimate against noise and transient fluctuations. The baseline trace was then interpolated across the full recording interval to generate a continuous estimate of F_0 (defined as the value under which P, percent of fluorescence values, fall in W, frame period). The top percentile values (50^{th} to 90^{th}) were used to calculate baseline of ASAP5 traces (fluorescence decreases in response to a voltage change) and inverted for all visual displays. Each sensor was imaged 2 days post transfection (with a media change at 24 h) and representative traces for three cells are shown in Figure 3.

Normalized fluorescence was calculated as $(F(t)-F_0(t))/F_0(t)$, where F(t) is the raw trace and $F_0(t)$ is baseline calculated with sliding window normalization at each time (t). Both raw and baseline traces were plotted for visual inspection, and normalized traces were displayed to quantify relative fluorescence changes (noting that the polarity is inverted for inverse indicators such as ASAP5). The normalized traces, raw traces, and calculated baseline fluorescence with accompanying window size and percentile settings are presented in Figure S8.

For comparison to Fluo-4 AM (Invitrogen, F14201), CMs were prepared and transfected as described above then incubated for 30 min with 2.5 μM Fluo-4 diluted in DMSO and 0.02% Pluronic™ F-127 (Invitrogen, P6866) in phenol-free RPMI (Gibco, 11835030). Cells were then washed once with phenol-free RPMI, allowed to equilibrate for 30 min at 37°C, then imaged in fresh phenol-free RPMI at 37°C on an epifluorescence microscope (a Lumencor SPECTRA X Light Engine on a Nikon Eclipse Ti-2 microscope) with a 20×0.80 NA objective (Nikon MRD70270) and ORCA-Fusion BT Digital CMOS camera (Hamamatsu C15440-20UP) controlled by NIS-Elements software. Fluo-4 was imaged with filter settings for 488 nm excitation and 521 nm emission with 50% illumination intensity and 9 ms exposure time. jRCaMP1b imaging was performed at 9 ms exposure time using Texas Red excitation

and filter settings (561 nm excitation and 609 nm emission) at 50% illumination intensity. Analysis was performed as described above using a window size 1 s and step size of 0.1 s.

Differentiation of hiPSCs to cardiomyocytes in suspension

hiPSC spheroids were differentiated according to manufacturer instructions for cardiomyocyte differentiation from PSC suspension culture in StemScale™ PSC Suspension Medium (ThermoFisher Scientific, A4965001).[80] Briefly, upon reaching an average diameter of between 250 μm and 300 μm (between 4 and 5 days), as assessed by brightfield or phase contrast microscopy, wells were washed with RPMI 1640 medium (ThermoFisher Scientific, 11875093) and incubated for 48 h in RPMI supplemented with B-27™ Supplement, minus insulin (ThermoFisher Scientific, A1895601) and 6 μM CHIR-99021 (Selleck Chemicals, S2924) (day 0). Exactly 48 h following CHIR-99021 addition (day 2), wells were washed with RPMI and incubated for 48 h in RPMI with B-27 minus insulin and 7.5 μM IWP-2 (Fisher Scientific, 35–331-0). Following IWP incubation (day 4), all wells were changed into RPMI with B-27 minus insulin for 48 h. On day 6, wells were changed into RPMI media supplemented with B-27™ Supplement (50×), serum free (ThermoFisher Scientific, 17504044). 50% media changes in RPMI with B-27 were performed every other day following day 6. All incubations were conducted at 37°C with 5% CO_2 on a plate shaker rotating at 70 rpm.

Fixation and immunofluorescent staining of cardiac spheroids

For cardiac spheroids, immunostaining was carried out at 24-well scale on day 14 and day 30 following differentiation induction at day 0. Cardiac spheroids were collected in an Eppendorf tube and kept on ice until fixation. Spheroids were allowed to settle by gravity sedimentation (~1 min) and were washed with 1 mL PBS prior to fixation for 30 min with Paraformaldehyde (PFA), 16% w/v aq. soln., methanol free (ThermoFisher Scientific, 043368-9 M) diluted to 4% in PBS with gently agitation. Following incubation, PFA was removed, and cardiac spheroids were washed for 5 min in PBS three times. Cardiac spheroids were then transferred to a 1% BSA (Millipore Sigma, A1595) coated 24-well plate and blocked with 1% BSA and 0.5% Triton X-100 (Merck, 108603 1000) in PBS for 2 h at room temperature or overnight at 4°C. Primary antibodies (mouse anti-cTnT – Abcam, ab8395; rabbit anti-nkx2.5 – Cell Signaling Technology, #8792) were diluted in 1% BSA in PBS according to manufacturer recommendations (1:1000) and added for 4°C with gentle agitation for 2 days. Secondary antibodies (goat anti-mouse 594 – Invitrogen, A11005; chicken anti-rabbit 647 – Invitrogen, A21443) were diluted to 1:200 and added after three 10-min washes with PBS. Following 2-day incubation at 4°C with gentle agitation, samples were washed three times with PBS and incubated overnight at 4°C with Hoechst (Thermo Scientific, #62249) diluted to 1:5000 in PBS. Samples were then washed and stored in PBS.

To measure apoptosis, cardiac spheroids were fixed and stained as described above with primary antibodies for cleaved caspase-3 (Abcam, ab32042) diluted at 1:500 and secondary antibody (Invitrogen, A21443) diluted 1:200 (Figure S12). Cleaved caspase-3 image analysis was performed using Fiji. Spheroids were masked on cleaved caspase-3 and eGFP signal using Otsu's automatic thresholding on maximum projections. Averages of eGFP positive and randomly selected pixels were calculated for comparison.

Quantification of labeling percentage in cardiac spheroids

Cardiac spheroids were fixed and stained as described above. 4-channel z-stacks were taken at a step size of 12.5 μm through the depth of spheroids using a spinning disk confocal (a Yokogawa CSU-W1 Confocal Scanner Unit on a Nikon Eclipse Ti microscope) equipped with a 4×0.2NA objective (Nikon MRD70040) and a Zyla PLUS 4.2 Megapixel camera controlled by NIS-Elements AR software. Hoechst: 405 nm excitation, 500 ms exposure time, 70.8 laser intensity; eGFP– 488 nm excitation, 300 ms exposure time, 100% laser intensity; NKx2.5–640 nm excitation, 100 ms exposure time, 100% laser intensity; cTnT – 561 nm excitation, 600 ms exposure time, 100% laser intensity.

Maximum intensity projections were generated for each image, and individual spheroids were segmented based on the Hoechst channel in Fiji. Briefly, images were split into individual color channels and maximum projections were generated. A manual threshold was set on the Hoechst channel to segment spheroids from background and was converted to a binary mask and 'analyze particles' was used to generate a set of individual ROIs that represent each spheroid. Spheroids that were negative for cTnT signal were manually excluded from analysis as not having undergone differentiation. The eGFP maximum projection was converted to 8-bit, and a histogram of pixel values was generated for each ROI with 256 bins. The percentage of pixels that were in bins 26 through 256 of each histogram out of the total number of pixels was used to represent the percentage of each spheroid that was eGFP positive.

Viability and metabolic health assessment in cardiac spheroids

On day 30 of cardiac differentiation of spheroids as described above, saRNA-eGFP transfected spheroids were transferred to untreated 6-well plates for staining. For viability staining, 20 μL of 1 mM stock of Calcein Blue, AM (ThermoFisher, C1429) diluted in DMSO was added to 10 mL PBS. Spheroids were incubated in dye solution for 30 min at 37°C and 70 rpm. Following incubation, spheroids were washed once with PBS then incubated an additional 30 min at 37°C and 70 rpm before being transferred into warmed phenol-free RPMI (Gibco, 11835030) for imaging. For metabolic health assessment, spheroids were incubated with CellROX orange (Invitrogen, C10443) used at a final concentration of 5 μM and MitoView 633 (Biotium, 70055) at a final concentration of 25 nM in RPMI 1640 (ThermoFisher Scientific, 11875093) with B-27 supplement (ThermoFisher Scientific, 17504044) for 30 min at 37°C and 70 rpm. Following staining, spheroids were washed twice with PBS then transferred into warmed phenol-free RPMI (Gibco, 11835030) for

imaging. Imaging was performed on a spinning disk confocal microscope (a Yokogawa CSU-W1 Confocal Scanner Unit on a Nikon Eclipse Ti microscope) equipped with a 10 × 0.45 NA (Nikon MRD70170) and a Zyla PLUS 4.2 Megapixel camera controlled by NIS-Elements AR software.

Calcein Blue, AM, CellROX orange, and MitoView 633 image analysis was performed using Fiji. For Calcein Blue, AM, spheroids were masked on Calcein Blue, AM and eGFP signal using Otsu's automatic thresholding on maximum projections. Averages of eGFP positive and randomly selected pixels were calculated for comparison. CellROX and MitoView analyses were performed the same way. Masks were used to segment spheroid volume in both the analysis and eGFP channel. Pearson and Spearman correlation calculations were performed between masked pixels in the CellROX/MitoView channel and eGFP.

Calcium imaging in cardiac spheroids

Calcium imaging in cardiac spheroids was performed at room temperature in RPMI 1640 medium (ThermoFisher Scientific, 11875093) B-27^{TM} Supplement (50×), serum free (ThermoFisher Scientific, 17504044) on a spinning disk confocal microscope (a Yokogawa CSU-W1 Confocal Scanner Unit on a Nikon Eclipse Ti microscope). Imaging was performed with a 4 × 0.2 NA (Nikon MRD70040), 10 × 0.45 NA (Nikon MRD70170), or 20 × 0.7 NA (Nikon MRH48250) objective, as specified in figure captions, using 561 nm excitation and Cy3 emission filter settings and 300 ms exposure time (3.33 Hz).

50 Hz imaging was performed at 37°C on an epifluorescence microscope (a Lumencor SPECTRA X Light Engine on a Nikon Eclipse Ti-2 microscope) with a 20×0.80 NA objective (Nikon MRD70270) and ORCA-Fusion BT Digital CMOS camera (Hamamatsu C15440-20UP) controlled by NIS-Elements software. Images were captured with 20 ms exposure time using Texas Red excitation and filter settings (561 nm excitation and 609 nm emission).

Calculation of calcium peak parameters in cardiac spheroids

In Fiji, an ROI was manually drawn to encompass regions of the image that showed changes in fluorescence and values were measured throughout the z stack (representing time). Each fluorescence time series representing calcium dynamics was analyzed using a custom MATLAB function (made available on GitHub). Briefly, raw traces consist of a time vector (t) and normalized fluorescence intensity values (y, scaled between 0 and 1 to account for differing baseline brightness to directly compare only temporal parameters). For acquisition rates lower than 30 fps (most taken at 3.33 Hz unless otherwise specified), traces were up-sampled by a piecewise cubic Hermite interpolation (pchip) to achieve an effective sampling frequency of >30 Hz. Peaks were identified using the findpeaks function with a minimum peak prominence threshold of 0.2 (out of 0–1) and a minimum inter-peak interval of 0.3 s. These plots were then displayed graphically to ensure accurate peak detection by visual inspection. For each 30 s trace, the total number of detected peaks was recorded. Inter-beat intervals (IBIs) were calculated as the time differences between successive peaks, and instantaneous beat frequencies were expressed as beats per minute (BPM = 60/IBI). Beat-to-beat variability was quantified as the coefficient of variation of the IBI (CV_IBI). Calcium traces with 2 or fewer identified peaks were removed from analysis since they falsely yield a coefficient of variation of 0. Because the original sampling interval imposes a quantization error ($0.3/\sqrt{12} \approx 0.087$ s based on the standard deviation of a uniform distribution), we estimated residual timing uncertainty after interpolation (0.02–0.03 s depending on SNR) which propagates to the estimated BPM uncertainty. For example, if peaks are detected 3 s apart, ±0.03 s results in ±1% uncertainty in BPM. Only for 50 Hz sampled traces were rise kinetics calculated (>10 frames per rise time without up-sampling) while decay kinetics (which last approximately 1 s) were calculated for all traces (points along observation curve are shown in Figure S11F). For the largest detected peak, the baseline was defined as the minimum fluorescence value preceding the peak. The 10%, 50%, and 90% fluorescence values relative to the peak amplitude were then computed. Rise time was measured as the time interval between the first crossing of the 10% and 90% fluorescence levels prior to the peak maximum. Decay was quantified as the time required for the signal to decrease from peak amplitude to 50% of the peak amplitude (T50) following the peak maximum. All extracted metrics were compiled for each trace.

Assessment of cardiomyocyte differentiation efficiency

hiPSCs were transfected with eGFP saRNA and differentiated into cardiomyocytes in 2-dimensional monolayers, then prepared for flow cytometry on day 15 of differentiation as previously described.[75] hiPSC-CMs were washed with PBS, then dissociated for 10 min using 0.25% Trypsin + EDTA at 37°C. Cells were fixed with 1% paraformaldehyde for 20 min at room temperature, then 90% ice-cold methanol for 15 min at 4°C. Cells were washed three times in 10% FBS in PBS, then blocked for 10 min in 10% FBS at room temperature. 1 million cells were aliquoted into individual Eppendorf tubes, then resuspended in 150 μL of 10% FBS with a 1:100 dilution of APC conjugated cardiac troponin T antibody, REAfinity (Miltenyi Biotec, 1C11) and incubated overnight at 4°C. Cells were washed with 10% FBS and resuspended in HBSS for analysis. Flow cytometry analysis was conducted on an LSR Fortessa Cell Analyzer using a 488 nm laser with a 530/30 filter for eGFP fluorescence and a 640 nm laser with a 670/30 filter for cTnT-APC fluorescence. FSC-A and SSC-A were used to gate cells, and eGFP$^+$ and cTnT-APC$^+$ gates were set using an untransfected and unstained negative control sample.

For analysis by immunofluorescence, hiPSC-CMs were dissociated on day 15 of differentiation using the STEMdiff Cardiomyocyte Dissociation Kit (StemCell Technologies, 05025) and plated onto a 96-well plate. Cells were allowed to recover for 3 days and then fixed with 4% paraformaldehyde for 15 min. Cells were then blocked and permeabilized with 2% BSA and 0.1% Triton X-100 in PBS for 1 h at room temperature, then incubated with primary antibody (rabbit anti-cTnT – ABclonal, A4914) at 1:1000 in 2% BSA overnight

at 4°C. Cells were washed three times with PBS and then incubated with secondary antibody (chicken anti-rabbit 647 – Invitrogen, A21443) overnight in 2% BSA. Samples were washed three times with PBS, incubated with Hoechst (Thermo Scientific, #62249) diluted to 1:5000 in PBS, and then washed and stored in PBS. Imaging was performed using the Operetta CLS High-Content Analysis System in confocal mode using a 40× water objective. Image analysis was performed using Fiji.

QUANTIFICATION AND STATISTICAL ANALYSIS

Each individual data point on summary graphs represents a biological or technical replicate and is specified as such in figure legends. Unless specified otherwise, data are reported as arithmetic means ± standard error of the mean (SEM) when reporting variation between averaged values and arithmetic means ± standard deviation when whole distributions are reported. Presented statistical analyses of normally distributed data include Welch's Student *t* test for pairwise comparisons and Ordinary one-way ANOVA with Bonferroni correction for multiple comparisons. Statistical comparisons of non-normally distributed data with two groups represent a Mann-Whitney U test. All calculations were performed using GraphPad Prism v.8 or MATLAB version 2023a, with significance set at ns: $p \geq 0.05$, *: $p < 0.05$; **: $p < 0.01$; ***: $p < 0.001$; ****: $p < 0.0001$.